Stray alternating current (AC) induced corrosion of steel fibre reinforced concrete

Abstract

This paper primarily discusses the assessment of stray DC and AC-induced corrosion phenomena on steel fibres and the analysis of the main influencing parameters. Instrumental methods in electrochemistry including Tafel polarization, Cyclic Potentiodynamic (CP) polarization and Electrochemical Impedance Spectroscopy (EIS) were used to assess the corrosion resistance of steel fibres which has great potential to replace conventional steel reinforcement in railway tunnel construction. The analytical model based on electric circuit modelling indicates that concrete containing discrete steel fibres has an inherent corrosion resistance to stray AC interference due to the electrical double layer developed on the surface.

Keywords

Steel fibre reinforced concrete

EIS

Cyclic voltammetry

Potentiostat

Galvanostat

Passivity

List of notations

A: Exposed anode area of a working electrode (cm^2)

β_a, β_b: Anodic and cathodic Tafel constants/gradients

C_f: Steel passive layer capacitance CPE ($S \cdot s^n \cdot cm^{-2}$)

C_{dl}:   Double layer capacitance CPE ($S \cdot s^n \cdot cm^{-2}$)

C: Capacitance (μF)

$E_{e,a}, E_{e,c}$:   Anodic and cathodic equilibrium potentials (V)

E_{corr}:   Corrosion potential (V)

E_0:   Amplitude of the AC potential (V)

E_{pass}:   Steel passivation potential (mV)

E_{pit}:	Steel pitting potential (mV)
E_{rep}:	Steel repassivation potential (mV)
f:	AC power supply frequency (Hz)
I:	Net electron flow of a circuit (A)
I_0:	Amplitude of the AC current (A)
I_a, I_c:	Anodic and cathodic currents (A)
I_{corr}:	Corrosion current (A)
i_{corr}:	Corrosion current density (A/cm^2)
$i_{r.m.s.}$:	Root-mean-square current (A)
i_s:	Stray current (A)
i_T:	Railway traction current (A)
i_{peak}:	Peak current density (A/cm^2) during the CP test
L:	Distance between adjacent railway substations (m)
$\eta_{e,a}$, $\eta_{e,c}$:	Anodic and cathodic overpotentials (V) from $E_{e,a}$ and $E_{e,c}$
R_s:	Resistance of the solution (Ω·cm^2 or Ω)
R_f:	Membrane resistance (Ω·cm^2 or Ω)
R_{ct}:	Charge transfer resistance of the steel (kΩ·cm^2 or kΩ)
r:	Ratio of the anodic and cathodic Tafel slopes ($r = \beta_a/\beta_c$)
r_R:	Running track resistance (Ω)
r_T:	track-earth resistance (Ω)
θ:	Phase shift (rad)
ω:	Angular velocity (rad/sec)

1. Introduction

Partly or completely concealed railway tunnels can effectively reduce noise and visual impacts during the construction and use of a railway. As a result, the £15bn Crossrail project consists of 26 miles of tunnels beneath built-up areas in London [1]; the £56 billion High-Speed 2 project contains 56 miles of tunnels which account for 47% of the total length [2]. The use of precast concrete lining elements in tunnel construction has been taken as standard practice to ensure its overall stability. For instance, over 200,000 concrete segments, each weighing over 3 tonnes, were used in the Crossrail project [1]. From a structural perspective, steel fibre reinforced concrete (SFRC) is an ideal substitute for conventional steel reinforcement in railway tunnel lining construction. SFRC has a greater compressive strength and a better fire resistance in comparison to ordinary steel reinforced concrete [3]. The use of SFRC can facilitate the concrete fabrication process by eliminating the need for constructing steel reinforcement cages, contributing to safe construction and a decreased construction cost. The latter is based on 95% of the material cost of a typical railway tunnel being taken by the concrete segmental linings; the cost of steel cage fabrication accounts for approximately 20-30% of conventional steel reinforced concrete [4]. These make railway tunnel lining construction a favoured application of SFRC. Despite these advantages, there is still a lack of knowledge concerning the susceptibility of stray current induced corrosion of SFRC, especially under a stray alternating current (AC) environment.

For an electrified railway, stray current refers to the electric current which disperses directly into the ground through the return path. The leakage of stray current to surrounding infrastructure including underground service cables, water mains and gas pipes can ultimately reduce their service life. In the UK, stray current induced corrosion is a long-recognized problem which led to a court judgment in 1893 (National Telephone Company versus Graff-Baker) [5]. It is a legal requirement for electrified railway and tramway promoters to demonstrate, mitigate and manage the stray current risk to a level that can be accepted by all parties who have concerns about their underground apparatus. The corrosive damage due to stray current will become more prominent in the UK as the government is committed to developing more electrified rail networks to provide sustainable and clean services for the public [6]. Previous investigations indicate that discrete steel fibres can pick up and transfer electric current under an externally applied direct current (DC) potential [3]. Stray DC-induced corrosion occurs where the electric current leaves the embedded steel fibre.

In comparison to the study of stray DC-induced corrosion, the investigation of stray alternating current (AC)-induced corrosion is very limited, despite that AC traction power systems account for 64% of the UK electrified railway network [7]. BS EN 15280 [8], evaluation of AC corrosion likelihood of buried pipelines, provides qualitative diagnosis for the evaluation of the likelihood of stray AC-induced corrosion and the AC current density was taken as a key parameter. For a stray DC interference alone issue, Bertolini et $al.$ [9] reported that a DC current density up to 1 mA/cm^2 was enough to initiate serious pitting corrosion in reinforced

concrete. In the second part of their work, the authors investigated the stray AC interference alone issue: an AC current density of 4 mA/cm^2 (50 Hz) did not initiate any corrosion in reinforced concrete containing up to 0.2% chloride (by mass of cement) [9]. Kuang and Cheng [10] investigated stray AC-induced corrosion of steel pipelines and reported that 20 mA/cm^2 (60 Hz) can be taken as the AC threshold current density for steel corrosion under a pH neutral environment. A higher AC threshold current density of 30 mA/cm^2 (60 Hz) is required under an alkaline environment (pH = 9.6). The authors used $NaHCO_3$ and Na_2CO_3 solutions to achieve electrolytes of different pH, i.e. 7.2 and 9.6. Brenna et $al.$ [11] presented similar results but using concrete as the electrolyte (pH ≥ 11.5): AC current densities lower than 10 mA/cm^2 (50 Hz) did not cause serious steel reinforcement corrosion under a chloride-free environment; the presence of a small amount of chloride, i.e. 0.25% by cement weight, increased the corrosion rate (CR) by one degree of magnitude. It should be noted that AC current densities may not be the only parameter governing AC-induced steel corrosion. Previous investigations on pipelines subjected to stray AC interference reported that the most rapid corrosion did not always occur in the places where the highest AC current density leakage was expected [12].

In order to quantitatively assess the kinetic parameters and their effects on the susceptibility of AC induced corrosion, Cao [13] developed a mathematical model for the prediction of the steel corrosion rate (CR) based on an anodic Tafel behaviour as illustrated in Eq. (1).

$$\eta_a = \text{E} - E_{e,a} = \alpha_a + \beta_a \ln I_a \tag{1}$$

Where η_a represents the anodic overpotential; β_a is the anodic Tafel constant. Anodic current due to the presence of AC can be determined as:

$$I_a = I_{corr} \cdot \exp(\frac{\Delta E}{\beta_a}) \tag{2}$$

Where I_{corr} is the corrosion current and $\Delta E = E_0 \cdot \sin \omega t$. E_0 represents the amplitude of the AC potential with an angular frequency ω (rad/sec). Through a Bessel function, Eq. (2) can be expanded as:

$$I_a = I_{corr} \cdot \sum_{n=0}^{\infty} \frac{\left(\frac{E_0}{2\beta_a}\right)^2}{(n!)^2} + I_{corr} \cdot \sum_{k=0}^{\infty} B \cdot \sin(2k+1)\omega t + I_{corr} \cdot \sum_{k=1}^{\infty} D \cdot \cos 2k\omega t \tag{3}$$

Both B and D are constant and contain E_0/β_a. A linear integration of I_a with respect to time (t) gives a total electric charge (coulombs), upon which the material loss and thus the CR can be calculated. As the second and third parts of Eq. (3) are periodic functions and their integrations over one period ($2\pi/\omega$) is zero, only the first part of Eq. (3) is responsible for the AC-induced corrosion and it is primarily affected by the magnitude of the AC potential applied (E_0) and the anodic Tafel slope (β_a). This conclusion was based on the assumption that the anodic half cycle during AC interference can be completely reversed during the cathodic half cycle. This however can lead to a flawed result as O_2 reduction or H_2 evolution is still more

favoured than the reduction reaction of steel ions during the cathodic half circle. It is therefore essential to consider anodic and cathodic half circles respectively to quantitatively assess AC-induced corrosion. Lalvani and Lin [14] proposed a revised mathematical model which can address both half cycles over one period. This was based on a root-mean-square current ($i_{r.m.s.}$) proposed:

$$i_{r.m.s.}^2 = \frac{1}{2\pi/\omega} \int_0^{2\pi/\omega} i^2 dt \qquad (4)$$

i represents the total current that flows through a circuit. The mathematical derivation, based on Tafel equation (Eq. (1)), indicates that $i_{r.m.s.}$ is primarily affected by the ratio of the anodic and cathodic Tafel slopes r ($r = \beta_a/\beta_c$). Bosch and Bogaerts [15] developed a mathematical model for the prediction of anodic current based on Butler-Volmer equation (Eq. (5)) which can consider a higher overpotential region in comparison to that of Tafel equation (Eq. (1)) and address different electrochemical models of the interfacial process.

$$I = I_a - I_c = I_{corr} \left[\exp\left(\frac{E - E_{corr}}{\beta_a}\right) - \exp(-\frac{E - E_{corr}}{\beta_c}) \right] \qquad (5)$$

An expansion through a modified Bessel function conducted by Bosch and Bogaerts [15] indicates that: 1) under both anodic and cathodic kinetically controlled processes, corrosion potential (E_{corr}) shifts to more negatively values when $r < 1$; the *CR* increases at any value of r; 2) under an anodic process kinetically controlled and a cathodic process controlled by both the kinetics of the interfacial charge transfer and mass transfer limited process of the reactants – the so called mixed (activation and diffusion) control, E_{corr} decreases with increasing AC voltage (E_0) and the extent of the decrease depends on the ratio of i_{corr}/i_L. i_{corr} represents the corrosion current density and i_L is the limiting diffusion current density of O_2 reduction [15]. Under both circumstances, the *CR* was independent of the angular velocity of the applied AC voltage (ω), despite a previous study shows that the *CR* is a strong function of ω [16]. This indicates that frequency dependent processes such as double layer charging cannot be disregarded as proposed by the authors in the above model. In addition to this, anodic and cathodic Tafel slopes (β_a and β_c) and their ratio (r) may change with time under an externally applied potential. It can lead to biased results when predicting i_{corr} by maintaining constant β_a and β_c values for a long period of time.

In addition to the analytical models discussed, a variety of electrochemical approaches have been developed for the assessment of AC-induced corrosion, such as a specially designed electrical circuit for the polarization measurement under an AC environment [11, 17, 18]. This circuit, as schematically shown in Fig. 1, allows both DC and AC currents to flow through the same test specimen (WE). The AC power supply provides periodically reversed electric current to simulate the AC interference; the potentiostat provides constant DC current through the same WE, allowing a standard DC polarization test to be conducted at the same time. Counter electrodes (CE) CE1 and CE2 respectively complete the AC and DC circuits. The

electric capacitor in the AC circuit prevents the interference of any DC current flows which may affect the corrosion measurement result; the DC circuit contains an electric inductor which effectively prevents AC current to flow into the potentiostat. There is however a systematic error in this experimental setup, even if the value of the inductor can be carefully decided to eliminate most of the AC current through the potentiostat. In this electrical circuit (Fig. 1), AC-induced corrosion mainly occurs on the side of the WE which is adjacent to CE1 while the DC polarization test provides corrosion information where the DC current leaves its anodically polarized side of the WE (adjacent to CE2). This will lead to an underestimate of the *CR* as the measurement is conducted on the other side of the specimen where AC-induced corrosion primarily occurs.
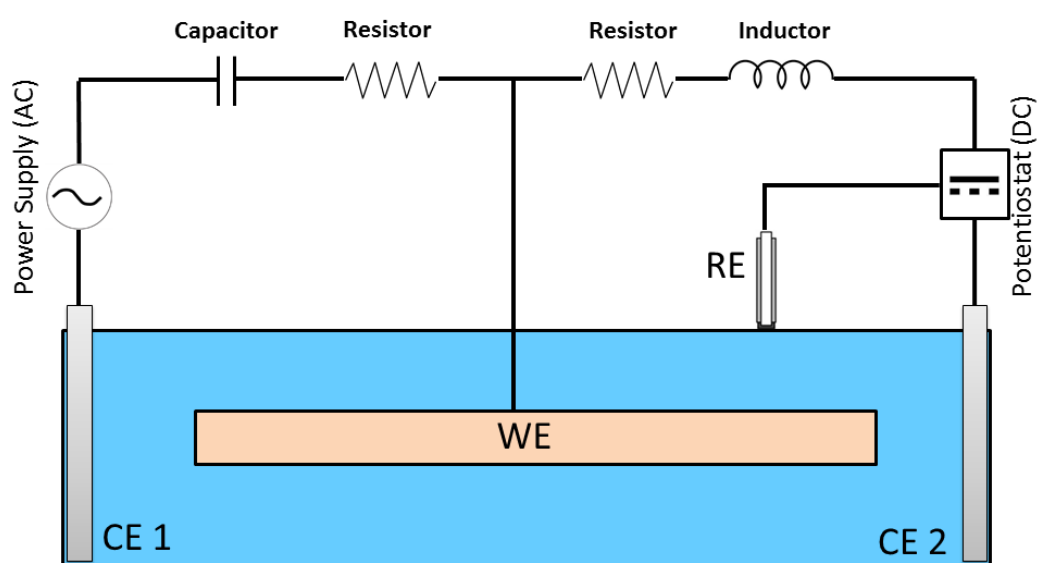
Fig. 1. Schematic of the electrical circuit designed for AC-induced corrosion measurement

In comparison to the electrical circuit shown in Fig. 1 which allows for separated DC and AC signals, an AC voltammetry technique allows AC-induced corrosion to be measured under a predominately DC environment. This is achieved by superimposing a small amplitude AC voltage perturbation (E_{AC}) on a DC potential (E_{DC}) during a potential sweep [16]. AC voltammetry provides useful information about the electrochemical double layer, in addition to the determination of the corrosion current density (i_{corr}) through interpreting E_{DC} and induced current (I) data. It should be noted that the amplitude of E_{AC} is usually less than 10 mV during AC voltammetry which might be insufficient to represent the effect of stray AC conditions. For a high-amplitude AC voltammetry test ($E_{AC} \geq 40$ mV), the peak non-Faradaic current (I_{AC}) was also found to be no longer dependent on the magnitude of the AC potential (E_{AC}) and this may prevent the use of high value E_{AC} to simulate a stray AC interference through AC voltammetry. This is according to the mathematical model developed and experimentally validated by Engblom *et al.* [19, 20]. During the experimental process, the authors [20] used two AC

potential amplitudes of 40 and 80 mV (35 Hz) which were respectively superimposed on a DC potential perturbation, ±200 mV (vs OCP).

In comparison to AC voltammetry, Electrochemical Impedance Spectroscopy (EIS) is based on an AC voltage perturbation without the presence of a DC potential. EIS can provide useful information about the double-layer capacitance which is related to the absorption and desorption processes during an electrochemical reaction [21]. EIS is usually conducted by applying a small sinusoidal potential, $E_0 \cdot \sin \omega t$, around the open circuit potential (OCP). OCP represents a constant offset potential between the WE and CE. A small magnitude of E_0 (e.g. ±25 mV vs OCP) is adopted to avoid any interference with the electrochemical reactions [3]. The electrochemical cell's current response is also sinusoidal but with a phase shift (φ), $I_0 \cdot \sin(\omega t + \varphi)$. It is engineering practice to interpret EIS data through equivalent electronic circuit modelling [22]. Wei *et al.* [23] proposed 4 electronic circuits to represent different steel-concrete interfacial conditions, e.g. from steel in a passive state to an accelerated corrosion process controlled by mass transfer, based on the EIS Bode Phase plot. This helps to address the change of the steel-concrete interfacial conditions as a result of the formation and breakdown of the steel passive layer. It should be noted that EIS alone may not be sufficient to model the effect of stray AC conditions due to the small magnitude of E_0, e.g. 25 mV. This may not be further improved by using a higher E_0. The corrosion potential (E_{corr}) may change under a higher E_0 and/or over a long period, which leads to polarization primarily in the anodic or cathodic regime, rather than providing information about the kinetics of the electrochemical process near E_{corr}. The pathway of the charged ions and electrons can also get complicated subjected to a high magnitude AC current when it involves both mass transport and electron transfers.

In addition to electrochemical approaches, other experimental approaches, involving laboratory controlled corrosion tests associated with Scanning Electron Microscope (SEM) analysis performed on samples' surface after tests end or at different stages of the tests, have been increasingly used to qualitatively evaluate generalized and pitting corrosion of steel. Goidanich *et al.* [24] observed a porous and weak layer of settlement developed on the surface of steel after an exposure to AC interferences through SEM. Wen *et al.* [18] reported an exponential relationship between steel corrosion pit numbers and AC current densities. There is however still a pressing need for the development of experimental approaches which are suitable to quantitatively assess the corrosion susceptibility of SFRC under stray AC conditions.

2. Experimental and analytical procedures

The primary objective of this project is to develop a suitable approach for the evaluation of the corrosion susceptibility of SFRC under a simulated stray DC or AC environment. Special attention was paid to the simulation of stray DC and AC interferences using laboratory equipment. Both potentiostatic (controlled electric voltage) and galvanostatic (controlled

electric current) polarization techniques have been previously used for the modelling of stray current [25-28]. The intensity of electrochemical processes strongly depends upon the electrode potential and anodic overpotential (η_a) is the major driving force for steel corrosion. It is therefore general practice to conduct a potential sweep to an electrode (e.g. steel) to obtain useful information about the kinetics of the electrochemical process such as polarization curves. Previous studies however indicate that corrosion potential (E_{corr}) may vary when the working electrode is exposed to stray currents [3]. This indicates that maintaining the same electrode potential over a long period time may not necessarily ensure that the same form (anodic or cathodic) and intensity of interference can be maintained. In this work, a galvanostatic (controlled electric current) polarization technique was developed for the modelling of stray AC current through laboratory experimentation. The adoption of this mode of control is in line with the field practicing, adopted in the community of railway operators, which uses to evaluate the stray current values by considering a linear relationship between the traction current and the stray current for a given section of the railway between two adjacent substations, according to the simplified model developed by Li [29]:

$$i_S = \frac{1}{12} i_T \frac{r_R}{r_T} L^2 \tag{6}$$

In this model, i_S represents the stray current (AC or DC) developed on a given section between two adjacent substations of the running tracks which proceeds as a return path to close the electric circuit; i_T represents the railway traction current; r_R is the resistance of the running tracks, r_T is track-and-earth resistance; L is the distance between nearby substations. The typical spacing between DC feeding substations (L) is about 2 km for a 750 V DC railway traction system and 3 to 4 km for a 1.5 kV DC or 15 kV AC traction system [30]; a standard track-and-earth insulation, compliant with EN 50122-2 [31], maintains constant track-and-earth resistance (r_T). The total stray current (whether DC or AC) developed on a given section between adjacent feeding substations of the running rail can therefore be determined according to track-and-earth resistance (r_T) and the distance between adjacent substations (L). This has been followed by the railway industry and a maximum average stray current of 2.5 mA/m is required to control stray current-induced corrosion of the running rail [31]. According to Eq. (6), an enhanced track-and-earth insulation (or r_T) can effectively reduce i_S. Charalambous *et al.* [32] successfully reduced i_S from 2.5 A to 50.3 mA by increasing r_T from 2 $\Omega{\cdot}$km to 100 $\Omega{\cdot}$km at a traction current of 1000 A (i_T). This also indicates that increased r_T, as a result of enhanced track-and-earth insulation and/or the use of discrete reinforcement in surrounding infrastructure, can mitigate but not eliminate the stray current. Anyhow and duly considering the above practical formula, as the traction current (i_T) is the leading parameter featuring any given electrified railway, it is considered here that the adoption of a stray current control mode is the most logical way of simulating the phenomenon.

In reinforced concrete, concrete performs as a solid electrolyte and its porous structure allows ions and molecules to come in contact with steel. In comparison to a solid electrolyte (e.g. concrete), an aqueous electrolyte is more cost effective and easier to prepare and manipulate [3, 33]. $Ca(OH)_2$, the major component in the concrete pore solution, is a strong electrolyte which provides ions to form cations and anions in the concrete pore solution when charged. In this project, 4 aqueous electrolytes were developed, including: saturated $Ca(OH)_2$; $Ca(OH)_2$ and 0.3 mol/L NaCl; $Ca(OH)_2$ and 0.6 mol/L NaCl; $Ca(OH)_2$ and 0.8 mol/L NaCl. Reagent grade NaCl was added into the simulated pore solution at different concentrations (0, 0.3, 0.6 and 0.8 mol/L or M). The latter (0.8 mol/L) represents the pore solution of concrete under a marine environment [34]. The permeation properties and porous structure of concrete were simulated using a high density upholstery foam beam, soaking up the simulated pore solution.

In this paper, Section 2.1 to 2.3 discuss the electrochemical analysis conducted using aqueous electrolytes. In order to verify that the results were applicable for solid electrolytes (e.g. concrete), mortar mixes were used as the solid electrolyte for EIS analysis and this is discussed in Section 2.4 and 2.5. The simulated stray AC interference test discussed in Section 2.5 also helps to justify whether discrete steel fibre can pick up and transfer stray AC currents.

All electrochemical tests discussed in this paper were conducted in an environmental chamber (Fig. 2) which performs as a Faraday cage. The exterior and interior parts of the environmental chamber were made from stainless steel and connected to earth, protecting the interior from electromagnetic interference from the outside. As steel corrosion is a thermally activated process and affected by the ambient temperature variations, the environmental chamber was set at a constant temperature (20°C) and humidity (90%) to ensure the reproducibility and repeatability of the experimental results.
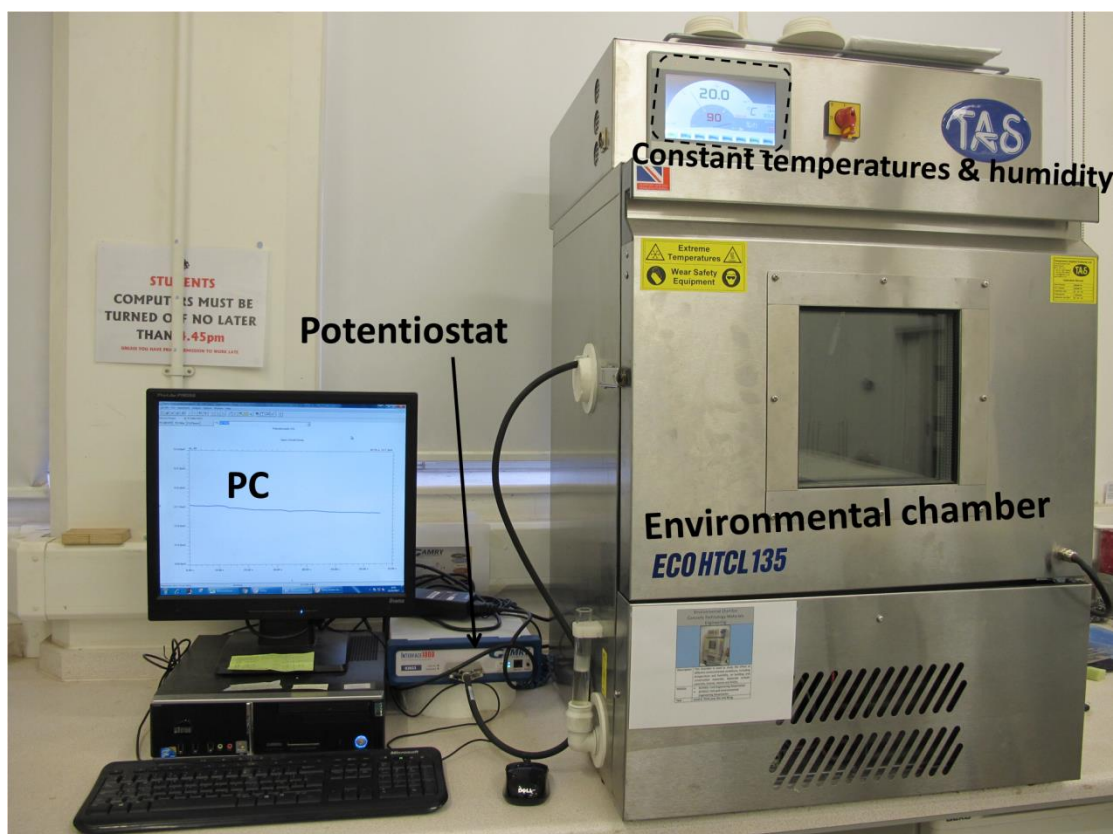
Fig. 2. Environmental chamber performs as a Faraday cage

2.1 Corrosion behaviour of steel fibres (aqueous electrolytes)

The steel fibre used in this work was provided in bags by Bekaert. This cold drawn low carbon steel fibre, 62 mm in length and 0.75 mm in diameter, has deformed ends and is adhered together by water reactive glue to facilitate concrete mixing. This water-soluble adhesive was carefully removed using deionized water and steel fibres were then dried under a room temperature (e.g. approximate 20°C). They were then ground by 2000 grit emery paper and rinsed in deionized water again prior to testing. All steel fibres were pre-connected to a copper cable (Fig. 3) to facilitate the electrochemical tests discussed later. The steel-copper connection was coated with hot melt polymer adhesive to prevent galvanostatic corrosion. This connection also provides an approximate exposed surface area 1.4 cm^2 of the WE (steel fibre) to the electrolyte. The conditions of the steel fibres achieved after this preparation procedure, i.e. when steel fibres are ready to be tested, are designated in the further text of this paper "as-received conditions".

Three instrumental methods for electrochemistry were adopted for the determination of the corrosion behaviour of steel fibres. These methods include Tafel polarization (Section 2.1.1), Cyclic Potentiodynamic (CP) polarization (Section 2.1.2) and Electrochemical Impedance Spectroscopy (EIS) tests (Section 2.1.3).
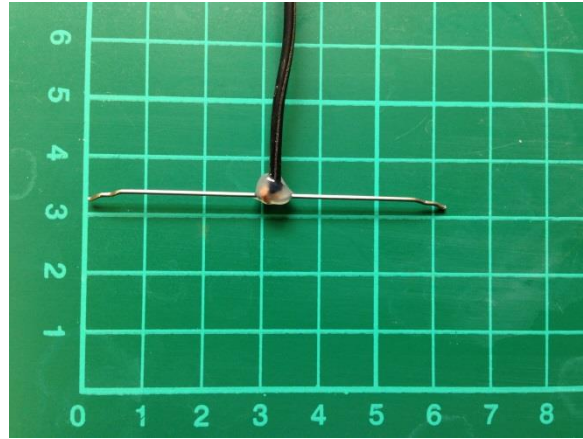
Fig. 3. Wired steel fibre protected with hot melt polymer adhesive

2.1.1 Tafel polarization test

A conventional 3-electrode electrochemical cell (Fig. 4) was developed for the Tafel polarization test using a Gamry Interface 1000E potentiostat. A steel fibre (Fig. 3) was used as the working electrode (WE) and its electrode potential was measured against a silver/silver chloride (Ag/AgCl) reference electrode (RE, with filling solution 3% KCl) which was placed on the top surface of the foam beam. During Tafel polarization, a DC potential perturbation, ±250 mV (vs OCP), was applied to the WE and the current flow between the WE and a 40×50×3mm graphite counter electrode (CE) was measured by the potentiostat at a slow potential scanning rate of 1 mV/sec. Such a potential range and scanning rate allows the nonlinear correlation between externally applied potential (E) and the current density i ($i = I/A$) response to be measured. Tafel slope analysis was then conducted to determine the corrosion current density (i_{corr}) and corrosion potential (E_{corr}) through a nonlinear regression and this is discussed in Section 3.1. The effect of chloride on the corrosion of steel fibres was investigated by adding NaCl into the electrolyte at different concentrations, i.e. 0, 0.3, 0.6 and 0.8 mol/L. Three parallel samples were prepared and tested in each group. Freshly prepared electrodes and electrolytes were used in each test.
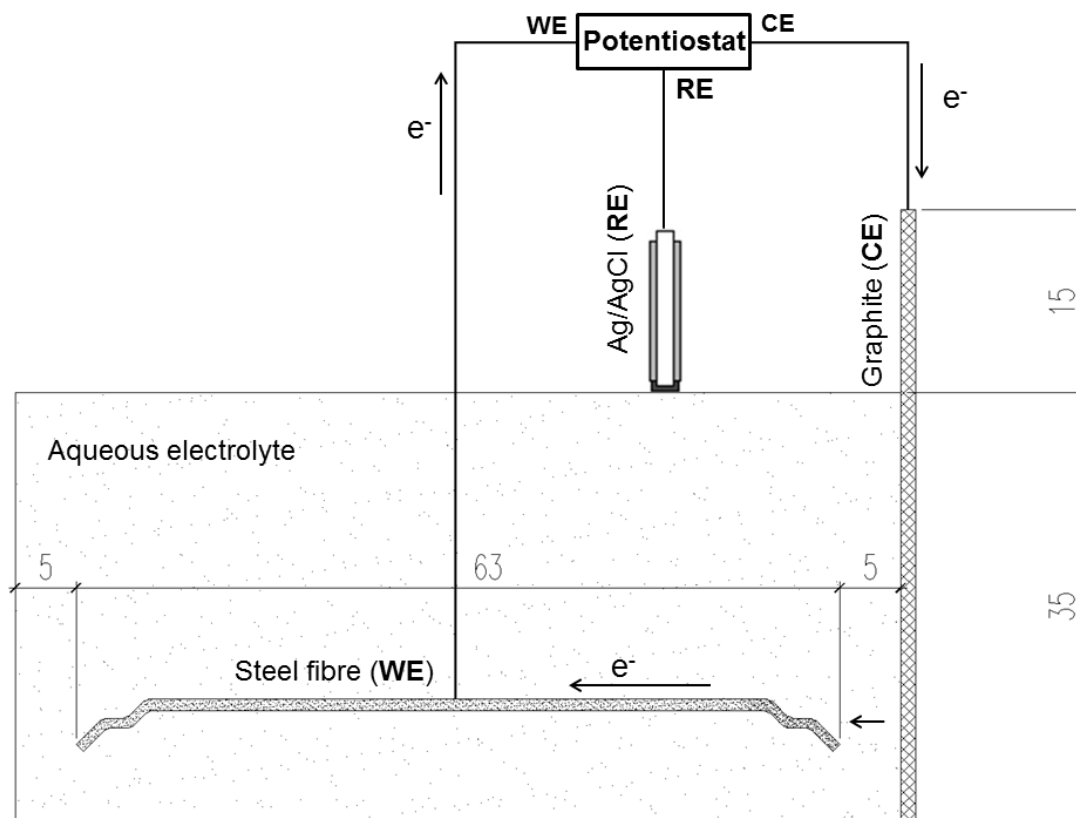
Fig. 4. 3-electrode Tafel polarization test (all units in mm)

2.1.2 Cyclic Potentiodynamic (CP) polarization test

Cyclic Potentiodynamic (CP) polarization was conducted to obtain additional information about the passivation behaviour of steel fibres subjected to a high overpotential value which can better simulate a stray DC environment. The experimental procedure of CP polarization was similar to that of Tafel polarization, despite the potential sweep being mainly along the anodic direction, e.g. -0.5 to 1.5 V from the open circuit potential (OCP). In comparison, a smaller potential perturbation, ±250 mV (vs OCP), was used during Tafel polarization. A faster scanning rate of 5 mV/sec was adopted in CP polarization and a reverse scan was conducted when either the maximum potential (i.e. 1.5 V vs OCP) or a maximum current density of 100 mA/cm^2 was achieved. CP polarization provides useful information about the steel pitting potential (E_{pit}) and peak current density (i_{peak}) which can be used to quantitatively assess the corrosion susceptibility of the steel fibre subjected to the simulated stray DC interference. Two samples were prepared and tested for each aqueous electrolyte composition simulating the concrete pore solution. Freshly prepared electrodes and electrolytes were taken at start of each test.

2.1.3 Electrochemical Impedance Spectroscopy (EIS)

The same 3-electrode electrochemical cell (Fig. 4) was used for the EIS test. After the preparation of the test cell, a conditioning time of 10 minutes was given to all samples,

allowing the open current potential (OCP) to be measured at a stabilized state. EIS was then conducted by sweeping a sinusoidal AC potential $E_0 \cdot \sin(\omega t)$ to the WE at frequencies varying between 10^5 and 10^{-1} Hz, with 10 measurements per decade or per order of magnitude and this process takes about 5 minutes. In comparison to Tafel and CP polarization, a reduced potential perturbation (E_0), ±25 mV (vs OCP), was adopted by EIS.

The impedance of the electrochemical cell was determined as the correlation between the applied potential (E) and the measured current (I). Three parallel samples were prepared and tested for each aqueous electrolyte composition simulating the concrete pore solution. Freshly prepared electrodes and electrolytes were taken at start of each test. The interpretation of EIS data was based on the best-fit results obtained through equivalent electrical circuit modelling and this is discussed in Section 3.1.

2.2 Stray DC-induced corrosion measurement (aqueous electrolytes)

Anodic overpotential (η_a) is the major driving force for steel corrosion. In this work, a galvanostatic polarization technique was developed based on the use of a 3-electrode electrochemical cell shown in Fig. 5. It allows DC voltage to be applied to the steel fibre under a controlled anodic current of 30 mA, which simulates the effect of a stray DC interference. As discussed previously, a higher stray current up to 50 mA is expected despite under high track-and-earth resistance [32]. The Gamry Interface 1000E potentiostat used in this study has a compliance voltage of 10 V which represents the maximum voltage (DC or AC) that the potentiostat can apply between the electrodes without causing a current overload. As a higher DC or AC current also causes a higher voltage drop between the electrodes, there is high possibility that the potentiostat may be overloaded, especially when high-resistance mortar is used as the electrolyte (Section 2.4). After a few trials, a controlled current of 30 mA was used in this work to simulate a stray DC interference. This was achieved by using the Gamry Interface 1000E potentiostat with the Gamry Physical Electrochemistry software package (PHE200). A sequence of measurements including 10-min stray DC interference test, EIS and Tafel polarization tests were conducted and this process was facilitated through programming using the Gamry's open source script language. EIS and Tafel polarization tests were conducted following the same procedure as discussed in Section 2.1 (Fig. 4). Freshly prepared electrodes and electrolytes were taken at start of each test. Three parallel samples were prepared and tested for each aqueous electrolyte composition simulating the concrete pore solution. Freshly prepared electrodes and electrolytes were taken at start of each test. Results are discussed in Section 3.2.
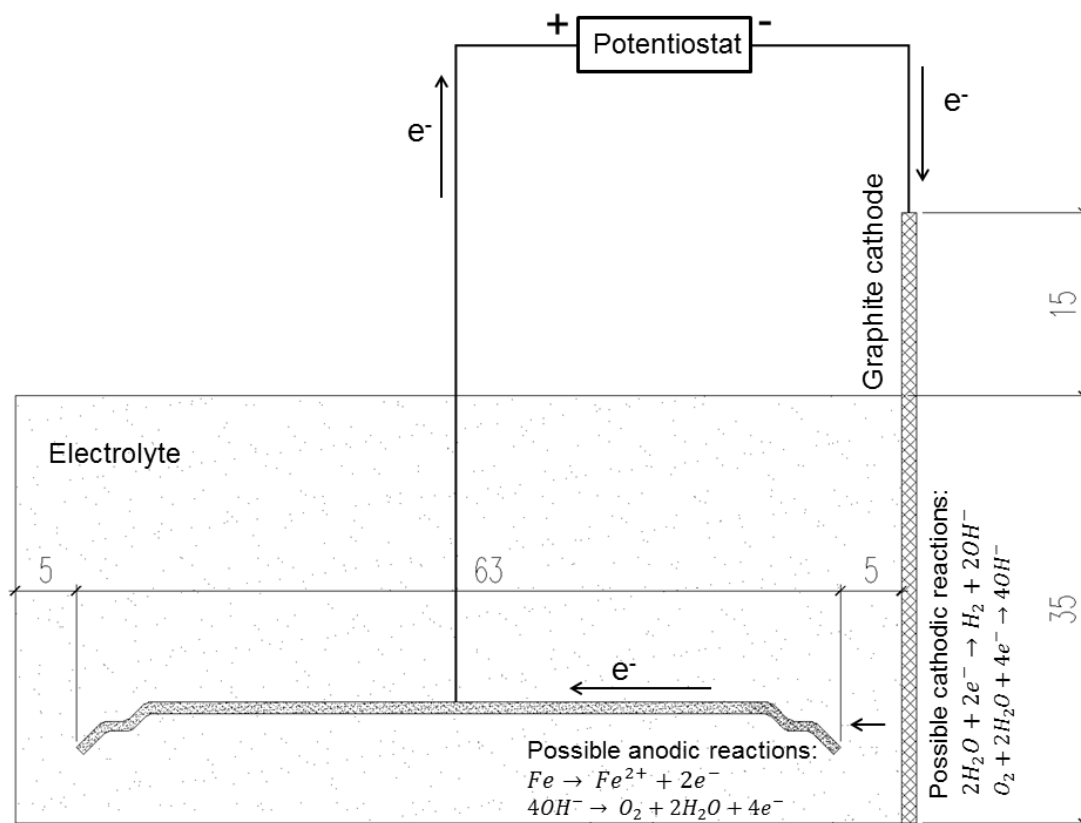
Fig. 5. DC galvanostatic polarization test (all units in mm)

2.3 Stray AC-induced corrosion measurement (aqueous electrolytes)

AC-induced corrosion is still a controversial subject, despite that AC traction power systems accounting for 64% of the UK electrified railway network [7]. In this work, a galvanostatic polarization technique was adopted using a similar electrochemical cell as seen in Fig. 5. It allows AC voltage to be applied to the steel fibre under a controlled anodic current of 30 mA (50 Hz), which simulates the effect of a stray AC interference. This was achieved using the Gamry Interface 1000E potentiostat with the Gamry's Virtual Front Panel (VFP600) software package which applied sine wave current perturbation of 30 mA to the WE (Fig. 5) at a constant frequency of 50 Hz, when the external potential (E) was measured. The AC frequency, i.e. 50 Hz, is the same as the UK National Grid AC frequency. After the 10-min stray AC interference test, EIS and Tafel polarization tests were conducted in sequence and results are discussed in Section 3.3. Three parallel samples were prepared and tested for each aqueous electrolyte composition simulating the concrete pore solution. Freshly prepared electrodes and electrolytes were taken at start of each test.

2.4 Stray AC-induced corrosion measurement (solid electrolytes)

In comparison to an aqueous electrolyte, a solid electrolyte such as concrete has different chemical compositions, electrical resistance and electronic structures. These can affect the corrosion behaviour of steel such as the passivation layer development. In order to verify that

the results obtained using aqueous electrolytes were applicable for SFRC, a 3-electrode electrochemical cell was developed as seen in Fig. 6. A steel fibre, pre-connected to a copper cable and coated with hot melt polymer adhesive, was embedded into freshly mixed mortar as the WE. This gives an exposed area of 1.4 cm^2 of the WE. Mortar is a mixture of cement, water and sand and the mix proportions used are shown in Table 1. The effect of chloride ions on the corrosion behaviour of SFRC was investigated by adding 0 and 2% NaCl (by mass of cement) into the mortar mixes. In comparison to mortar, concrete also contains coarse aggregate such as granite and gravel. The possible effect of coarse aggregate on the corrosion of steel fibres is an on-going area of research. Two graphite plates, 40×50×3 mm, were placed on both sides of the WE as the counter electrode (CE). Such a twin-graphite CE system ensures a more uniform transmission of electrical signals between the WE and CE. The gap between WE and CE was maintained as 5 mm. An Ag/AgCl reference electrode (RE) was placed near the WE to reduce solution resistance (R_s). A sponge soaking saturated Ca(OH)$_2$ solution was placed between the RE and mortar, ensuring a good electrical connection between the RE and the solid electrolyte.

One sample was prepared and tested for each of the two mortar mixes containing 0 and 2% NaCl (by mass of cement). Freshly prepared electrodes and electrolytes (mortar) were used at start of each test.   All mortar specimens were placed in the environmental chamber (Fig. 2) set at 20 °C and 90% humidity. The effect of a stray AC interference on the corrosion of SFRC was investigated at the age of 3 days after casting. This was achieved using the Gamry Interface 1000E potentiostat with the Gamry's Virtual Front Panel (VFP600) software package which applied sine wave current perturbation of 30 mA (50 Hz) between the WE and CE for up to 4 hours. EIS was conducted in each hour, i.e. 0, 1, 2, 3 and 4 hours, at a frequency ranging from 10^5 Hz to 0.1 Hz with a ±25 mV potential perturbation around the OCP. The interpretation of EIS data was based on the best-fit results obtained through equivalent electrical circuit modelling and this is discussed in Section 3.4.
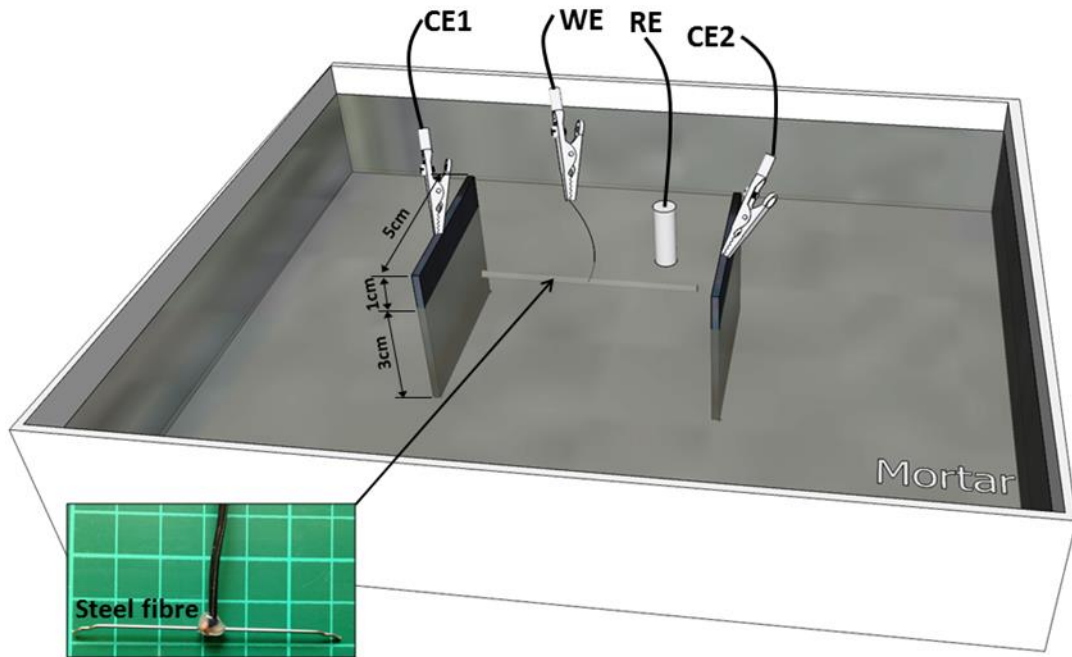
Fig. 6. SFRC AC corrosion test

Table 1 Mortar mix proportions

Mortar mixes	CEM I 52,5 (kg/m^3)	Free W/C	Sand (0-4mm) (kg/m^3)	NaCl (kg/m^3)
0%NaCl	480	0.35	1814	0
2%NaCl	480	0.35	1814	9.6

2.5 Test of discrete steel fibre to pick up and transfer stray AC current (solid electrolytes)

In order to justify whether a discrete steel fibre can pick up and transfer AC currents, a 24-hr stray AC interference test, as seen in Fig. 7, was conducted. A steel fibre, pre-connected to a copper cable and coated with a hot melt polymer adhesive, was embedded into freshly mixed mortar. The mix proportions are shown in Table 1. The effect of chloride ions on the corrosion behaviour of SFRC was investigated by adding 0 and 2% NaCl (by mass of cement) into the mortar mixes. Two graphite plates, 40×50×3 mm, were placed on both sides of the WE as the auxiliary electrode. One sample was prepared and tested for each of the mortar mixes containing 0 and 2% NaCl (by mass of cement). Freshly prepared electrodes and electrolytes (mortar) were taken at start of each test. The AC stray current interference test was conducted on the age of 3 days after casting.

The Gamry Interface 1000E potentiostat with the Gamry's Virtual Front Panel (VFP600) software package allows the potentiostat to perform as a galvanostat which drives a constant AC current ($I = I_0 \cdot \sin \omega t$; $I_0 = 10 \, mA$; $\omega = 50 \, Hz$) between two auxiliary graphite electrodes

for 24 hours, simultaneously measuring voltage drop between the steel fibre and the graphite auxiliary graphite electrode. An increased AC voltage in comparison to that used in Fig. 6 is expected to maintain the same current value (e.g. 30 mA, 50 Hz) due to the increased solution resistivity (on both sides of the embedded steel fibre) alongside the maturity of mortar. Through a few trials, a reduced controlled AC current value of 10 mA (50 Hz) was used to avoid overloading the potentiostat which has a compliance voltage of 10V.

After the 24-hr simulated AC stray current interference test, Electrochemical Impedance Spectroscopy (EIS) was conducted: the embedded steel fibre was used as the working electrode (WE) and an Ag/AgCl reference electrode (RE) was placed on the top of the steel fibre. A potential perturbation (E_0), ±25 mV (vs OCP), was adopted and a sinusoidal AC potential $E_0 \cdot \sin(\omega t)$, at frequencies varying between 10^5 and 10^{-1} Hz, was swept between the WE and two graphite electrodes (CE). The impedance of the electrochemical cell was determined as the correlation between the applied potential (E) and the measured current density (i). The interpretation of EIS data was based on the best-fit results obtained through equivalent electrical circuit modelling and this is discussed in Section 3.5.
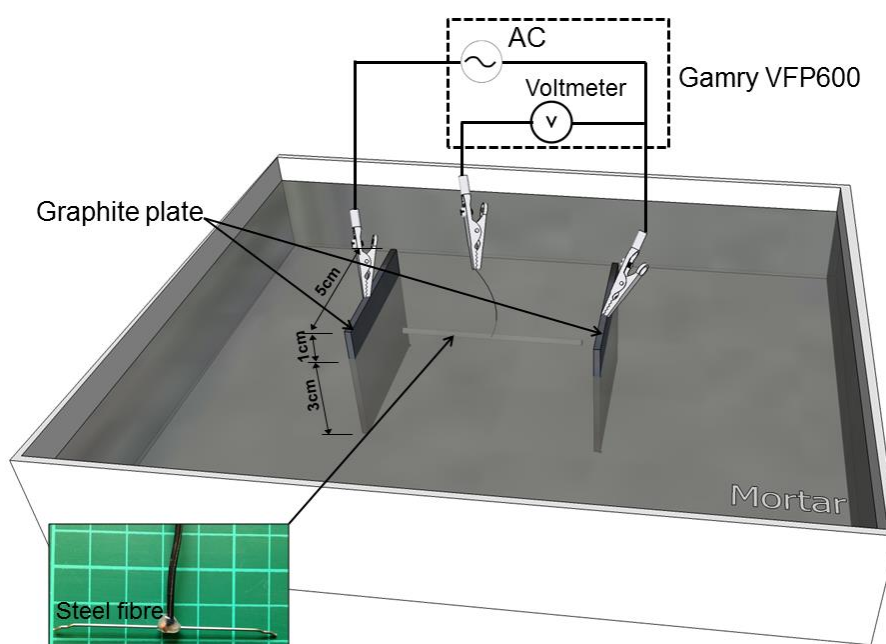
Fig. 7. 24-hr simulated stray AC interference test

3. Results and discussion

3.1 Corrosion behaviour of steel fibres (as-received conditions)

In this work, three instrumental methods for electrochemistry were adopted for the assessment of the corrosion behaviour of steel fibres. Tafel polarization provides useful information about steel fibres under a small potential perturbation, ±250 mV (vs OCP). Tafel polarization results are presented as curves between the electrode potential E (vs Ag/AgCl RE) and the current density i ($i = I/A$) on a logarithmic scale (Fig. 8). A represents the exposed surface area of the steel fibre to the electrolyte, i.e. 1.4 cm^2. A nonlinear regression

analysis based on Butler-Volmer equation (Eq. (5)) was conducted to determine i_{corr} and corrosion potential (E_{corr}) using the Gamry Echem Analyst software package [35]. The best-fit results for i_{corr} and E_{corr}, as seen in Fig. 9, indicate that E_{corr} shifted to more negative values due to the presence of NaCl in the electrolyte. Alongside a reduction in E_{corr}, i_{corr} increased steadily from 5.4 μA/cm^2 under a chloride-free environment to 72.2 μA/cm^2 with 0.8 mol/L NaCl in the electrolyte, indicating serious steel corrosion. This also shows the presence of chlorides, especially at high concentrations ($\geq$ 0.6 mol/L), seriously enhanced steel fibre corrosion.

In contrast to Tafel polarization which was conducted at an equilibrium state (near E_{corr}), Cyclic Potentiodynamic (CP) polarization provides useful information about the passivation behaviour of steel fibres due to a higher overpotential value applied. Such a high overpotential (i.e. 1.5 V vs OCP) can be taken as a simulation of a stray DC interference. CP voltammograms (Fig. 10) show a constant current density (i) with an increase of E and this can be defined as a passivation potential, E_{pass}. With a further increase of E, i increases again in conjunction with the breakdown of the steel passive layer. Thereafter, i increases sharply from the pitting potential (E_{pit}) where the disruptive effect of NaCl overcame the stabilizing effect of OH$^-$ [36]. Through comparing Fig. 10 (a) and (b), E_{pit} was found to reduce significantly with even 0.3 mol/L NaCl in the electrolyte, showing an earlier breakdown of the steel passive layer. During the reverse scanning, the repassivation potential, E_{rep}, was identified. E_{rep} was found to be close to E_{corr}, showing that the damage to the steel passive layer was not repairable, with and without the presence of NaCl [36]. The presence of NaCl however significantly increased the peak current density, i_{peak}. Fig. 10 (a) shows that i_{peak} was less than 10 mA/cm^2 under a chloride-free environment when the potential swept to 1.5 V (vs OCP). With only 0.3 mol/L NaCl in the electrolyte, i_{peak} reached 60 mA/cm^2 as seen in Fig. 10 (b), showing a serious anodic dissolution. Through comparing the Tafel and CP polarization results, it can be concluded that a small amount of NaCl (0.3 mol/L), which in itself may be insufficient to cause severe corrosion in SFRC in absence of any electrical interference, may still be sufficient to significantly increase the corrosion risk under a stray DC environment.

EIS was conducted on steel fibres at their as-received conditions. In comparison to Tafel and CP polarization, EIS can be taken as a non-destructive approach due to the small AC perturbation (e.g. ±25 mV vs OCP) applied. EIS results are presented as the Bode phase plot (Fig. 12 (a)), Bode $|Z|$ plot (Fig. 12 (b)) and Nyquist plot (Fig. 12 (c)). The Bode phase plot allows the phase shift angle (θ) to be plotted in comparison to the excitation frequency (Hz) on a logarithmic scale. It shows that the phase angle (θ) dropped gradually at low frequencies between 0.1 and 10 Hz with up to 0.3 mol/L NaCl in the electrolyte. The lowest value (valley) was reached at an excitation frequency of approximate 10 Hz. This indicates that the steel passive layer might have been locally destroyed and pitting corrosion might have occurred according to Wei $et\ al.$ [23]. With 0.6 and 0.8 mol/L NaCl in the electrolyte, the phase angle (θ) dropped constantly at low frequencies until the lowest value (valley) was reached at an

excitation frequency of approximate 100 Hz, indicating the rate of charge transfer increased and the mass transfer might have become a key parameter governing the corrosion rate [23].

The Bode $|Z|$ plot allows the absolute values of the impedance ($|Z|$) to be plotted against the logarithm of frequency (Hz). It shows that $|Z|$ drops significantly from approximate 10,000 $\Omega \cdot cm^2$ at an excitation frequency of 0.1 Hz to less than 30 $\Omega \cdot cm^2$ at 10^5 Hz. $|Z|$ obtained at the high frequency (10^5 Hz) represents the bulk resistance of the solution (R_s) which is much smaller than the charge transfer resistance (R_{ct}). This finding agrees with the Nyquist plot: the real impedance (Z') within the high frequency region (10^5 Hz) is 80 $\Omega \cdot cm^2$ which can be attributed to the low solution resistance (R_s) aqueous electrolyte used.

Based on above interpretations of the EIS data, an equivalent circuit (Fig. 11) was developed to represent the corrosion state experienced by the steel fibres. It consists of solution resistance (R_s), membrane resistance (R_f, i.e. resistance of any film layer present at sample surface and exerting a resistance towards charge transfer at interface) and charge transfer resistance (R_{ct}). R_{ct} and R_f define the difficulty of a kinetically controlled electrochemical reaction. The equivalent circuit also contains the capacitance of the steel passive layer (C_f) and electrical double layer (C_{dl}) which were modelled as a constant phase element (CPE). In comparison to a standard capacitor, CPE can better simulate the surface roughness and heterogeneousness of a double layer [33]. Best-fit curves obtained from one sample based on the equivalent electronic circuit modelling are shown in Fig. 12 and they match very well with the measured EIS data. The average results obtained from three parallel samples are presented in Table 2. Fig. 13 and Table 2 indicate that the presence of NaCl in the electrolyte significantly reduced R_{ct}: R_{ct} reduced by almost one degree of magnitude from 15 k$\Omega \cdot cm^2$ to 2.4 k$\Omega \cdot cm^2$, with 0.8 mol/L NaCl added into the electrolyte, showing high susceptibility for steel corrosion. Table 2 also shows that R_f gradually increased with an increase of the chloride content, alongside a major increase of C_f. This indicates that porous and non-protective corrosion products have been developed on the steel surface. This, in conjunction with the reduction in R_{ct}, shows that the presence of NaCl led to enhanced corrosion in steel fibres. This finding agrees with the best-fit results for C_{dl} which increased steadily and was over 85×10^{-6} $S \cdot s^n \cdot cm^{-2}$ with 0.6 mol/L NaCl in the electrolyte, indicating that generalized corrosion might have occurred on the steel fibre surface [33, 36].

In summary, Tafel polarization provides useful information about electrochemical kinetics relating to the corrosion rate (*CR*) where the values of polarization are low. The presence of a small amount of NaCl (0.3 mol/L) increased i_{corr} and thus the *CR* although the detrimental effect is deemed to be insignificant, according to the Tafel polarization results. EIS provides useful information about the steel polarization resistance which can be used to assess the corrosion resistance of steel under low-value polarization. A significant reduction of R_{ct} at high NaCl concentrations ($\geq$ 0.6 mol/L) indicates serious corrosion reactions on the steel surface. CP polarization results, especially those obtained at high-value anodic overpotential, indicates

that the presence of even a small amount of chlorides (0.3 mol/L) can significantly reduce the corrosion resistance of steel fibres, in addition to its detrimental effect on the development of steel passivation layer. These however cannot be sufficiently considered by low-value polarization techniques including Tafel polarization or EIS tests.
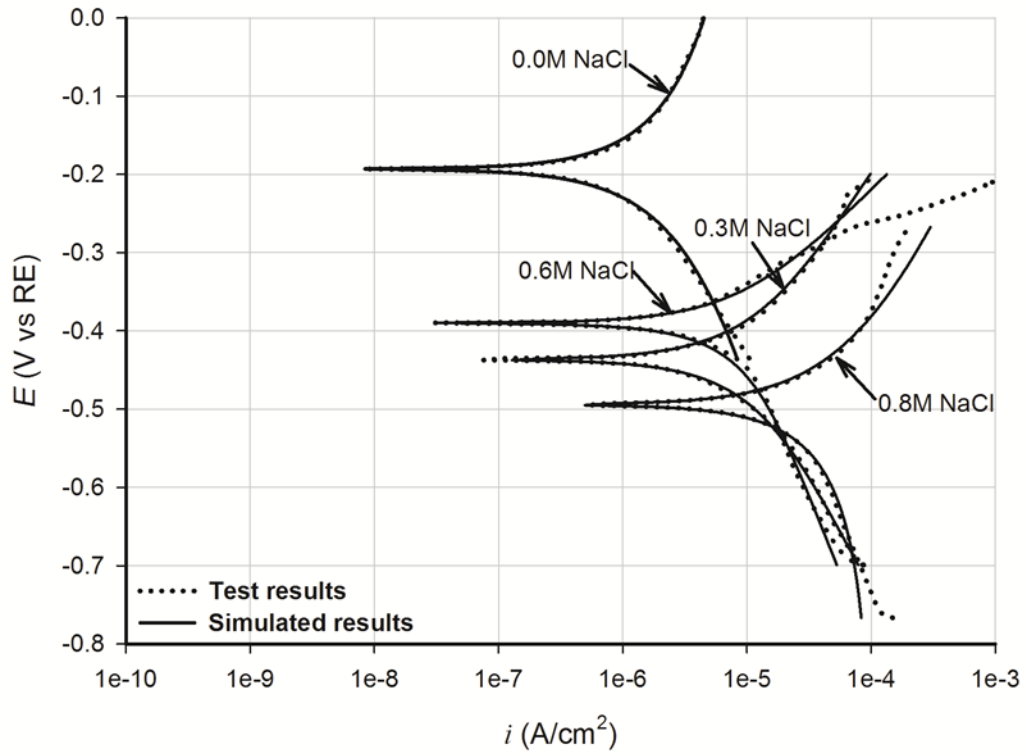

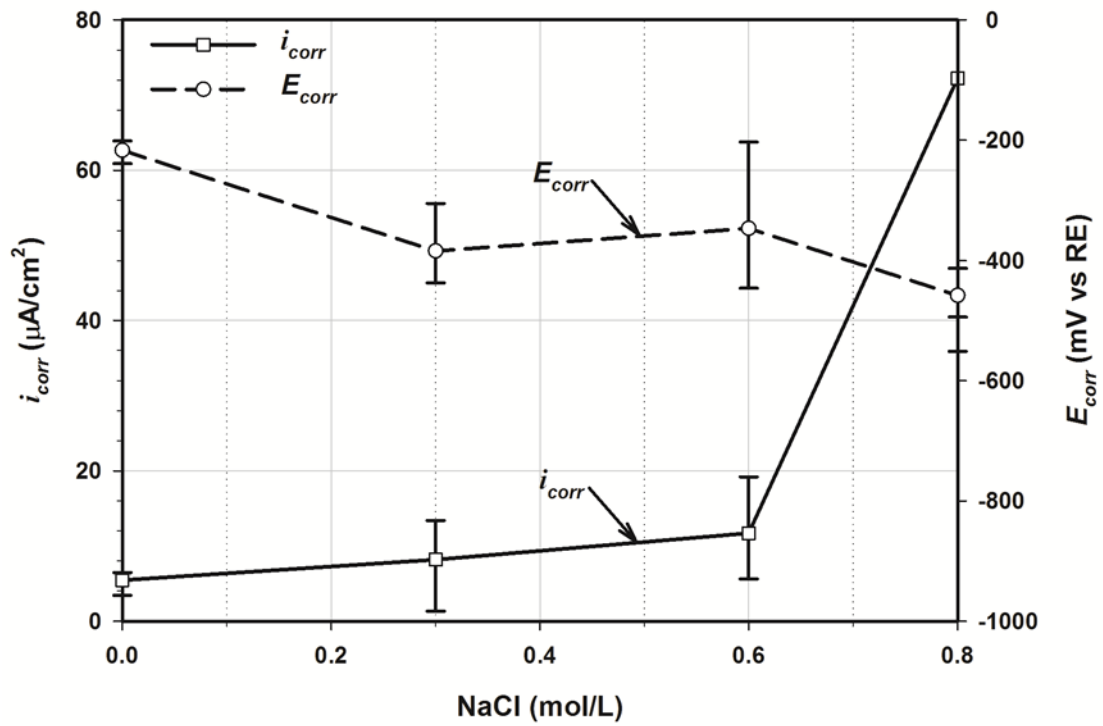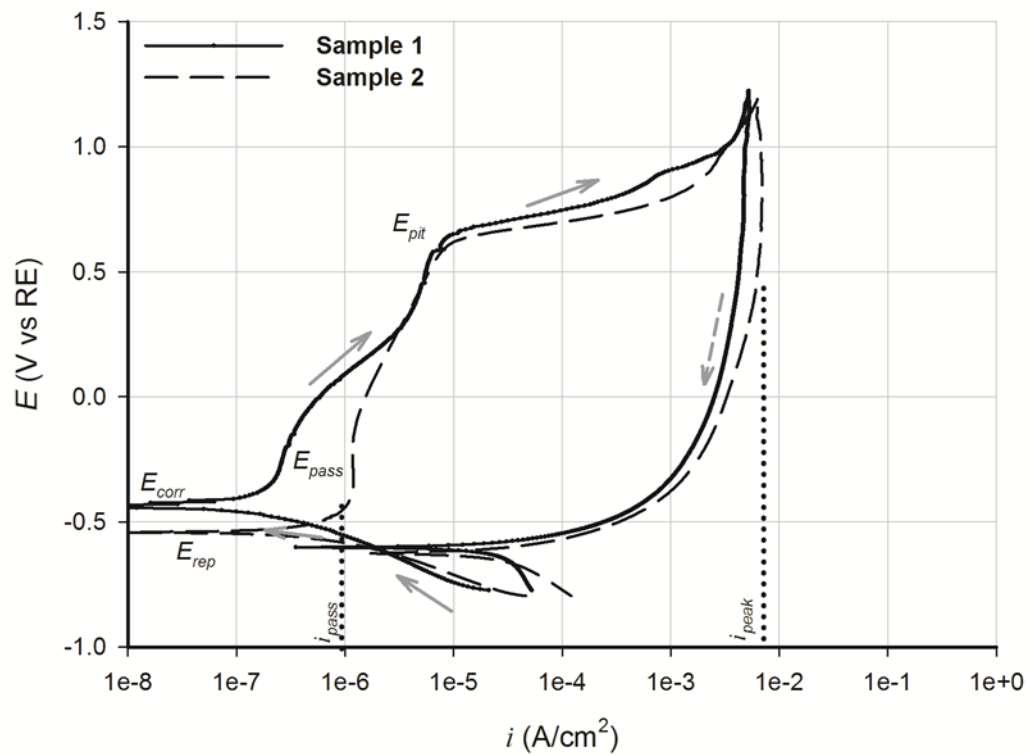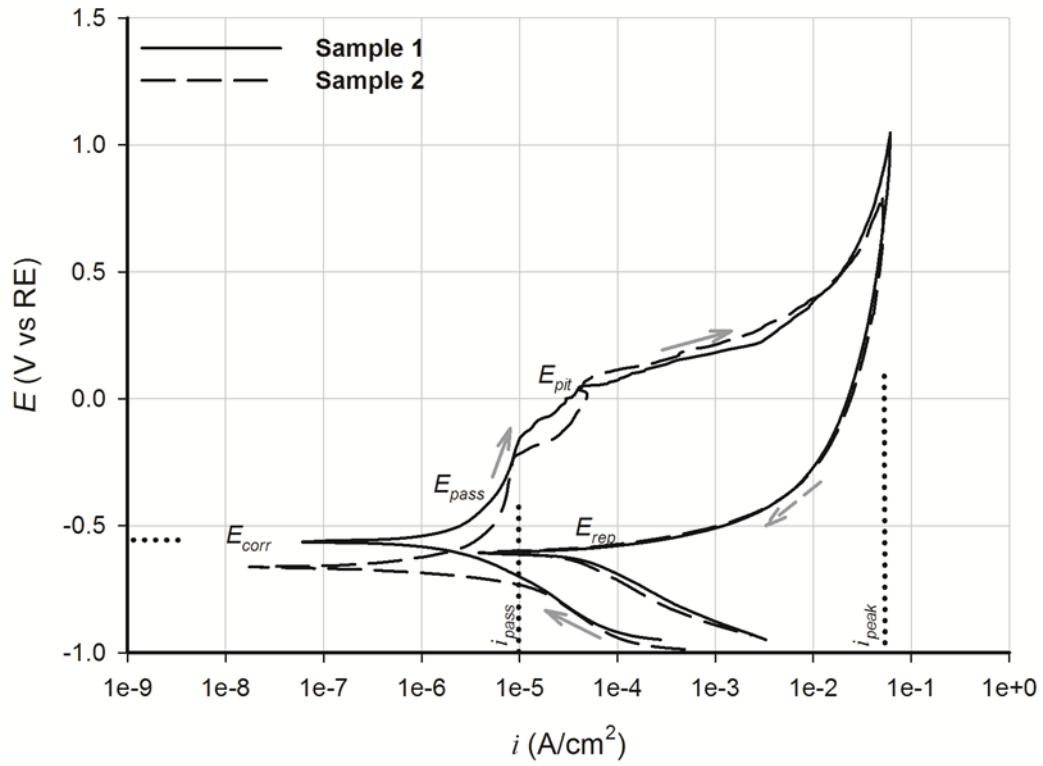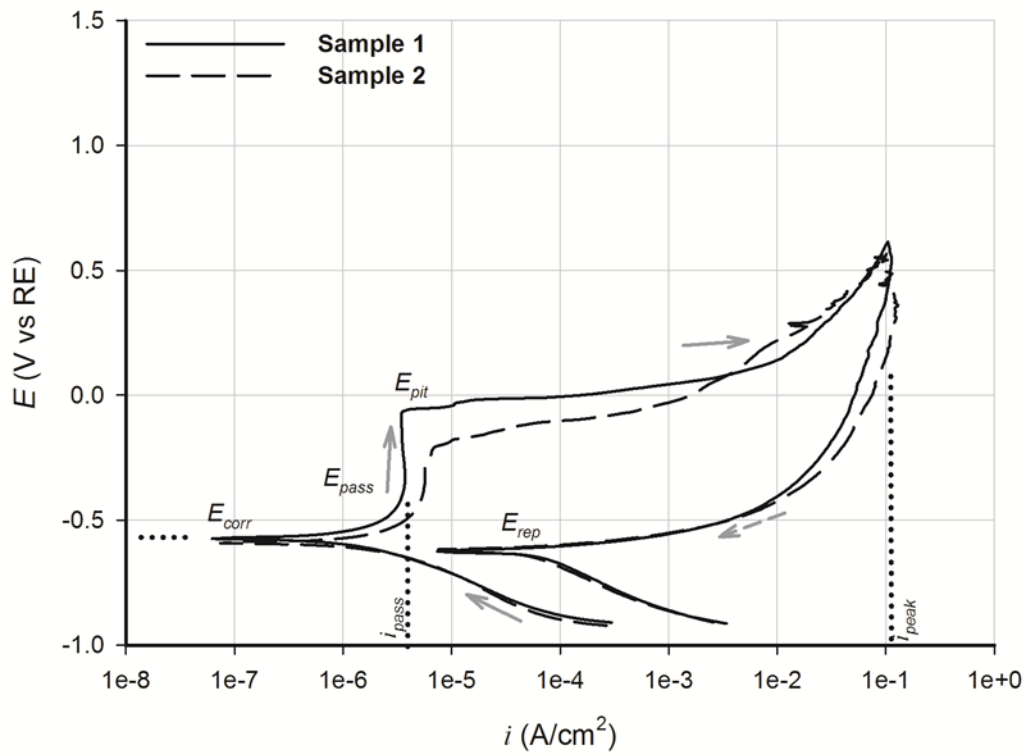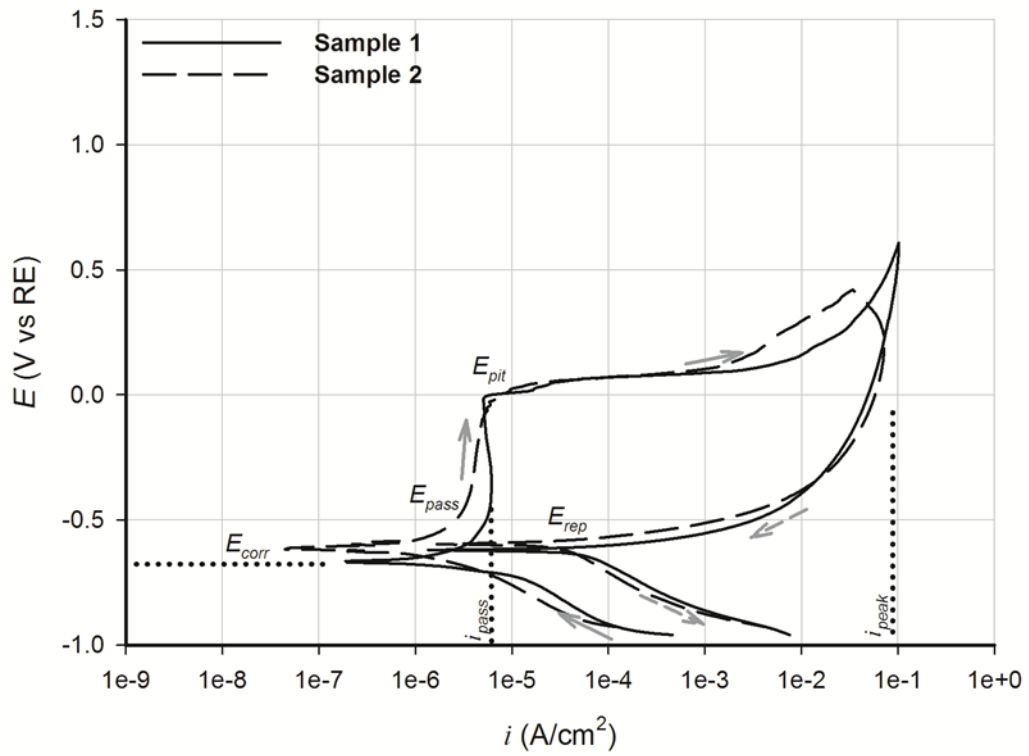Fig. 8. Tafel polarization results (as-received conditions)

Fig. 9. Tafel polarization results (as-received conditions)

(a) 0.0 mol/L NaCl in the electrolyte

(b) 0.3 mol/L NaCl in the electrolyte

(c) 0.6 mol/L NaCl in the electrolyte

(d) 0.8 mol/L NaCl in the electrolyte

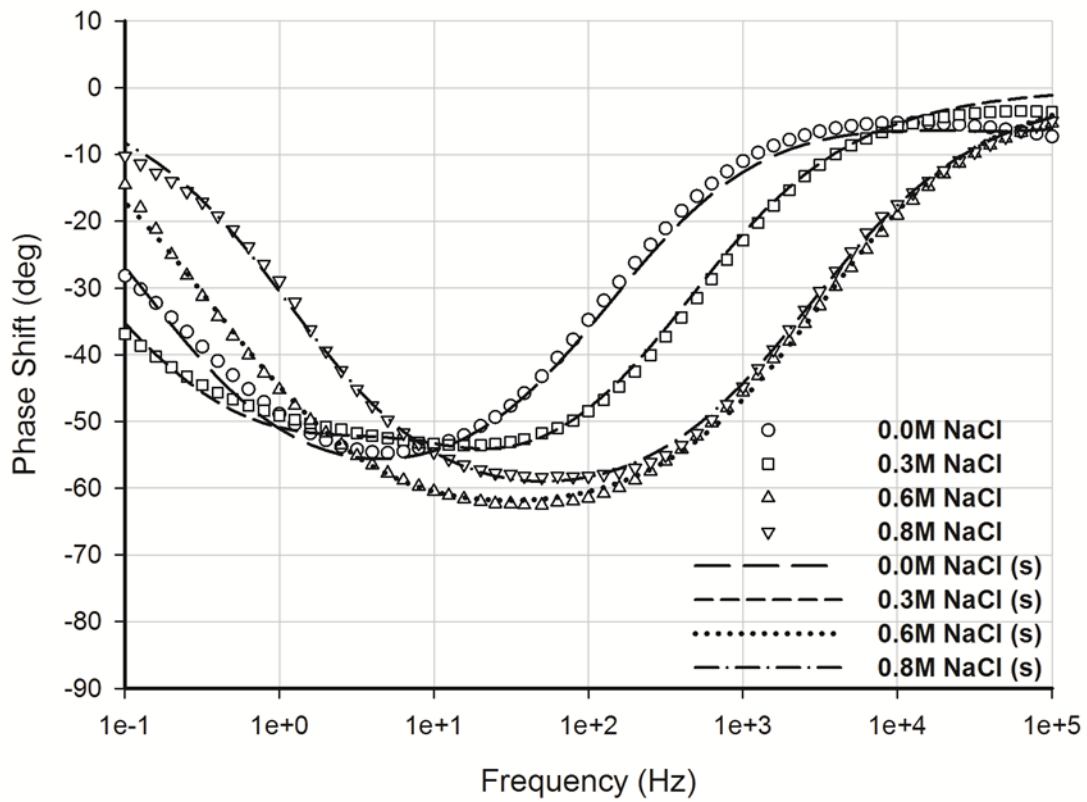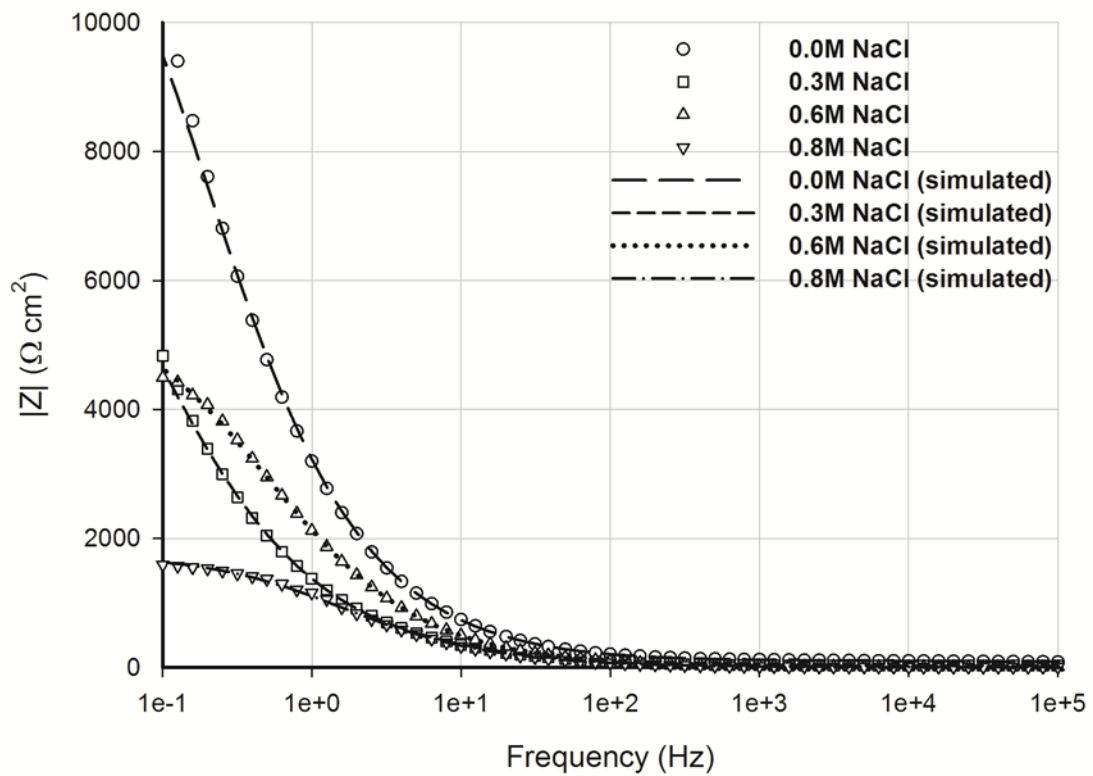Fig. 10. CP polarization test results (as-received conditions)
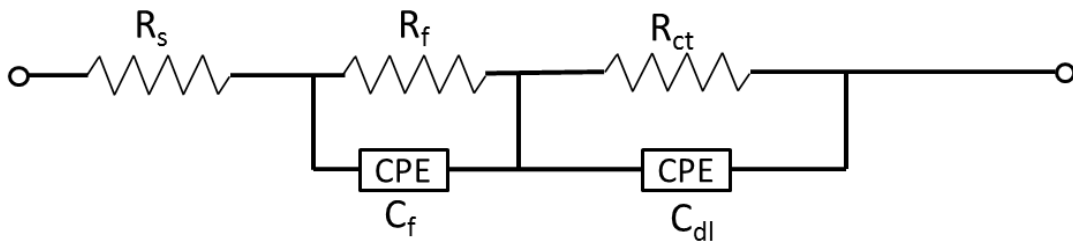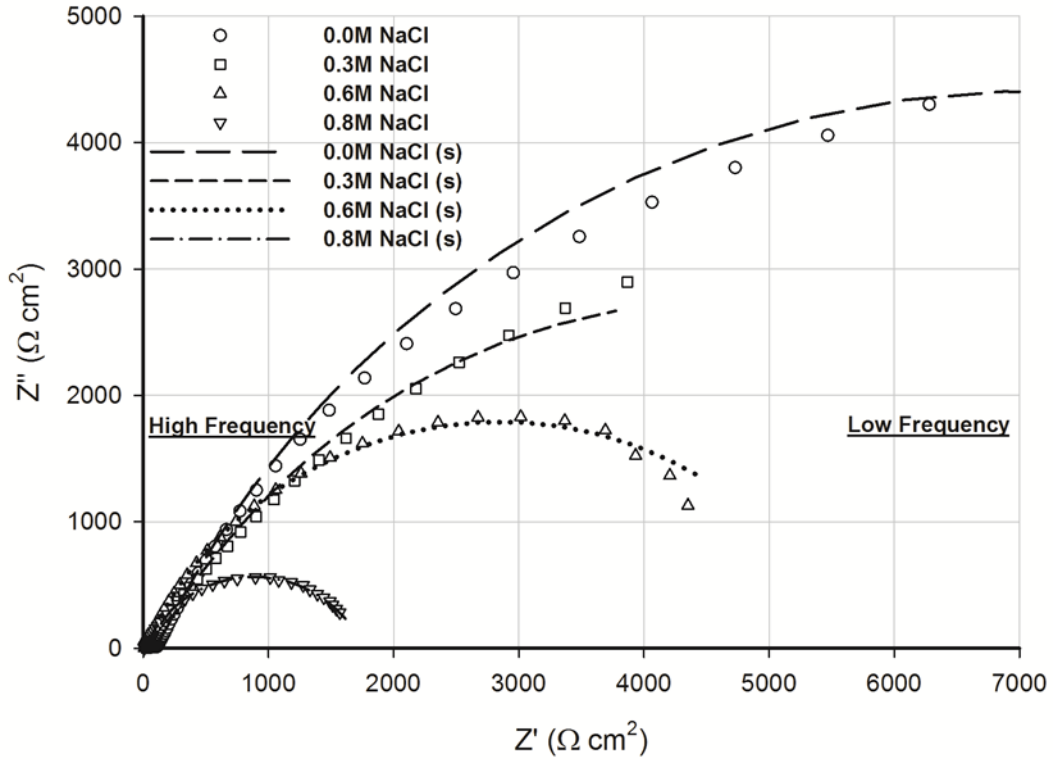

Fig. 11. EIS equivalent electrical circuit

(a) Bode phase plot

(c) Nyquist plot

Fig. 12. EIS measurements and best-fit curves (as-received conditions)

Table 2 EIS best-fit results (as-received conditions)

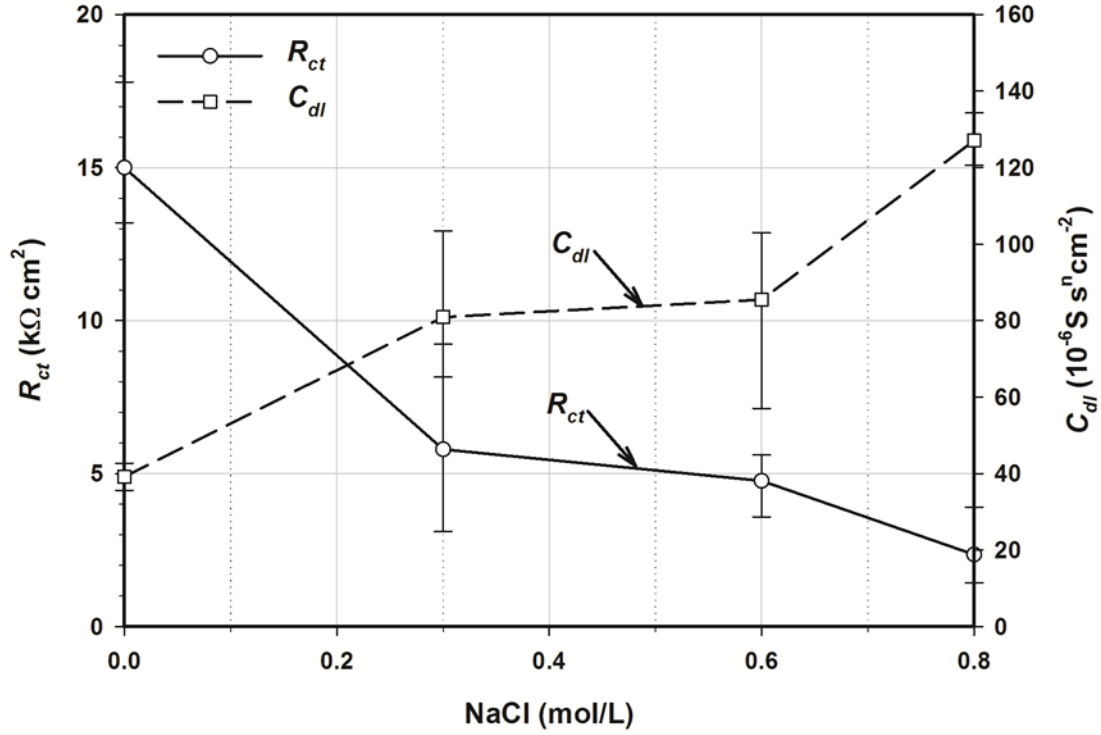|	OCP	R_s	R_f	C_f	n_f	R_{ct}	C_{dl}	n_{dl}
	(mV)	($\Omega \cdot cm^2$)	($\Omega \cdot cm^2$)	($10^{-6}S \cdot s^n \cdot cm^{-2}$)		($k\Omega \cdot cm^2$)	($10^{-6}S \cdot s^n \cdot cm^{-2}$)	
0.0 mol/L NaCl	-197	2.9	40.6	0.3	0.70	15.0	39.1	0.78
0.3 mol/L NaCl	-401	8.9	47.1	294.5	0.41	5.8	81.0	0.73
0.6 mol/L NaCl	-453	7.4	80.5	547.0	0.60	4.8	85.5	0.70
0.8 mol/L NaCl	-475	9.2	88.4	682.0	0.52	2.4	127.1	0.75

Fig. 13. EIS best-fit results (as-received conditions)

3.2 Corrosion behaviour of steel fibres after stray DC interference

During the stray DC interference test, an external DC voltage allows charged anions and cations in the electrolyte to flow throughout the bulk solution, as shown in Fig. 5. The potential difference between the WE and the bulk solution induces the exchange of electrons and as such, an electric current is pushed through the entire electrolytic cell. In addition to the metallic iron oxidation, the other possible anodic reactions involved include:

$$2Cl^- \rightarrow Cl_2 + 2e^- \tag{7}$$

$$4OH^- \rightarrow O_2 + 2H_2O + 4e^- \tag{8}$$

$$2H_2O \rightarrow O_2 + 4H^+ + 4e^- \tag{9}$$

An external DC voltage also provides the free energy required for the coupled cathodic reactions, such as:

$$2H_2O + 2e^- \rightarrow H_2 + 2OH^- \tag{10}$$

$$O_2 + 2H_2O + 4e^- \rightarrow 4OH^- \tag{11}$$

Upon anodic stray current interference, chloride oxidation to chlorine gas (Eq. (7)) would happen in a chloride environment and they will prevail the slow kinetically controlled half-cell reactions associated with O_2 evolution (e.g. Eq. (8) and (9)). At the CE, H_2O and O_2 reduction

26

reactions (Eq. (10) and (11)) are both expected from an energetic point of view. However, the reduction of O_2 can be hindered due to the low solubility of O_2 in water [37].

Fig. 14 indicates that the exposure of steel fibres to an anodic stray DC current interference for 10 min shifted E_{corr} towards more negative potentials, in comparison to the results obtained when Tafel polarization was performed without any prior stray DC interference (Fig. 9). Steel fibres still demonstrated a high corrosion resistance with up to 0.6 mol/L NaCl added into the electrolyte, as the i_{corr} values obtained via Butler-Volmer regression analysis are similar to those obtained without pre-exposure to the DC interference (Fig. 9). The combined effect of the simulated stray DC current and high-concentration chloride (0.8 mol/L NaCl) however significantly increased i_{corr} and thus the CR: i_{corr} was over 100 $\mu A/cm^2$, indicating high corrosion susceptibility. These findings agree with the EIS results shown in Fig. 15 and Table 3 (EIS best-fit results). A significant reduction of R_{ct} and an increase of C_{dl} was noted due to the presence of NaCl in the electrolyte, together with the Tafel polarization results for these concentrations, indicate possible serious generalized corrosion on the steel fibre surface. Visual observation was conducted to assess the steel fibre surface after the stray DC interference test. A black corrosion product was observed on the steel fibre surface and this can be attributed to the formation of magnetite (Fe_3O_4) due to a deficiency of O_2 at the steel surface [38]. The chemical composition assessment of the corrosion product is an area where ongoing research is undertaken.
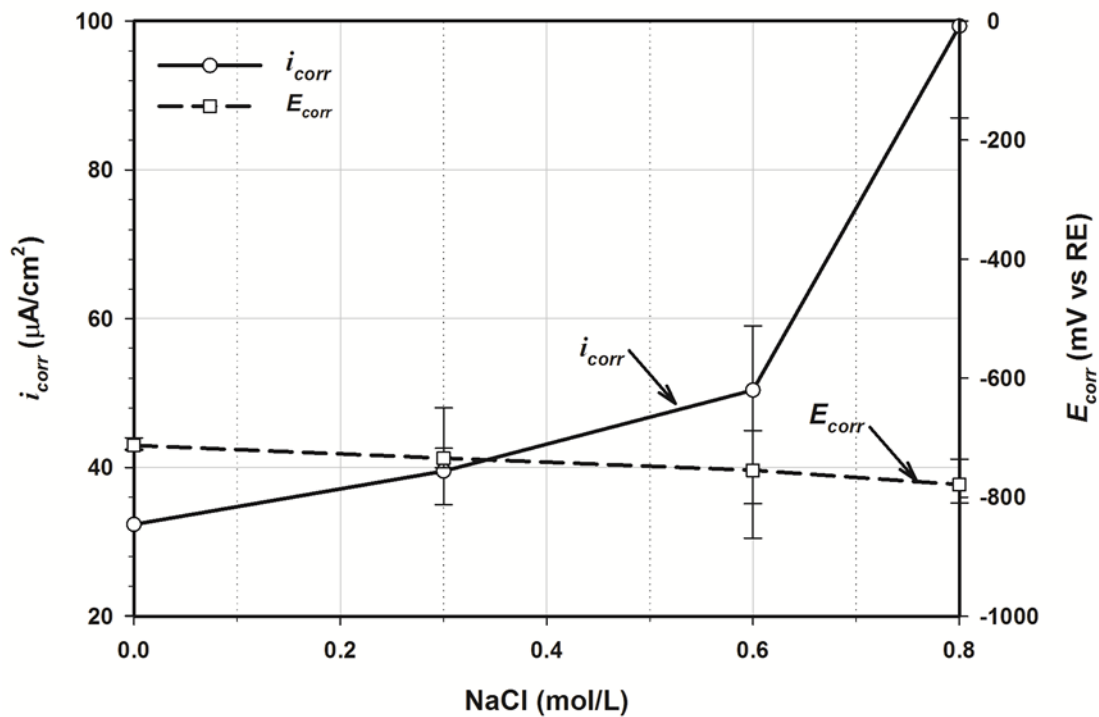

Fig. 14. Tafel polarization results (after 10-min stray DC interference)
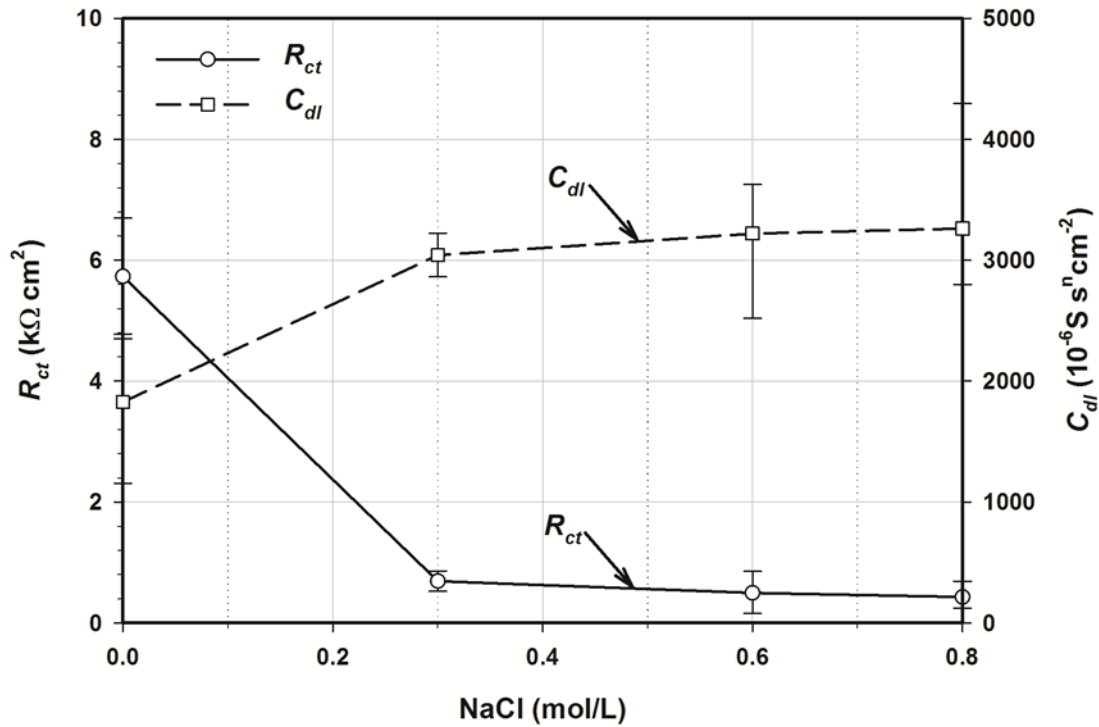
Fig. 15. EIS best-fit results (after 10-min stray DC interference)

Table 3 EIS best-fit results (after 10-min stray DC interference)

	OCP (mV)	R_s ($\Omega \cdot cm^2$)	R_f ($\Omega \cdot cm^2$)	C_f ($10^{-6}S \cdot s^n \cdot cm^{-2}$)	n_f	R_{ct} ($k\Omega \cdot cm^2$)	C_{dl} ($10^{-6}S \cdot s^n \cdot cm^{-2}$)	n_{dl}
0.0 mol/L NaCl	-580	7.3	156	600	0.40	5.7	1825	0.98
0.3 mol/L NaCl	-613	8.2	249	738	0.90	0.7	3043	0.78
0.6 mol/L NaCl	-631	17.2	13.2	772	0.86	0.5	3221	0.86
0.8 mol/L NaCl	-629	7.1	234	812	0.22	0.4	3264	0.85

3.3 Corrosion behaviour of steel fibres after stray AC interference

The stray AC interference test, although of the same current amplitude (30 mA for an exposed area of 1.4 cm^2) as the stray DC interference test, led to different Tafel polarization and EIS test results (Fig. 16 and Fig. 17). Fig. 16 indicates that the pre-exposure of steel fibres (prior to carrying out the Tafel polarization procedure) to a simulated AC stray current interference in form of a sinewave current perturbation, shifted the corrosion potential E_{corr} towards more negative values, in comparison to the results obtained when the Tafel polarization procedure was applied to the steel fibre in its "as-received conditions" as seen in Fig. 9. This agrees with results reported in the literature [17, 39]. The presence of AC interference however did not significantly increase i_{corr} when comparing the case where the Tafel polarization procedure was carried out on the as-received steel fibre (Fig. 9) with the case where it was performed after the exposure of the steel fibre to the simulated AC stray current interference. This finding was also confirmed by the EIS best-fit results (e.g. R_{ct}) as

seen in Table 4. CP polarization results (Fig. 18) also shows that similar CP voltammograms were obtained before and after the AC exposure with 0.3 mol/L NaCl added into the electrolyte. Visual observation was conducted to assess the steel fibre surface after exposure to the simulated AC stray current interference: no rust was observed on the steel fibre surface with even 0.8 mol/L NaCl in the electrolyte.
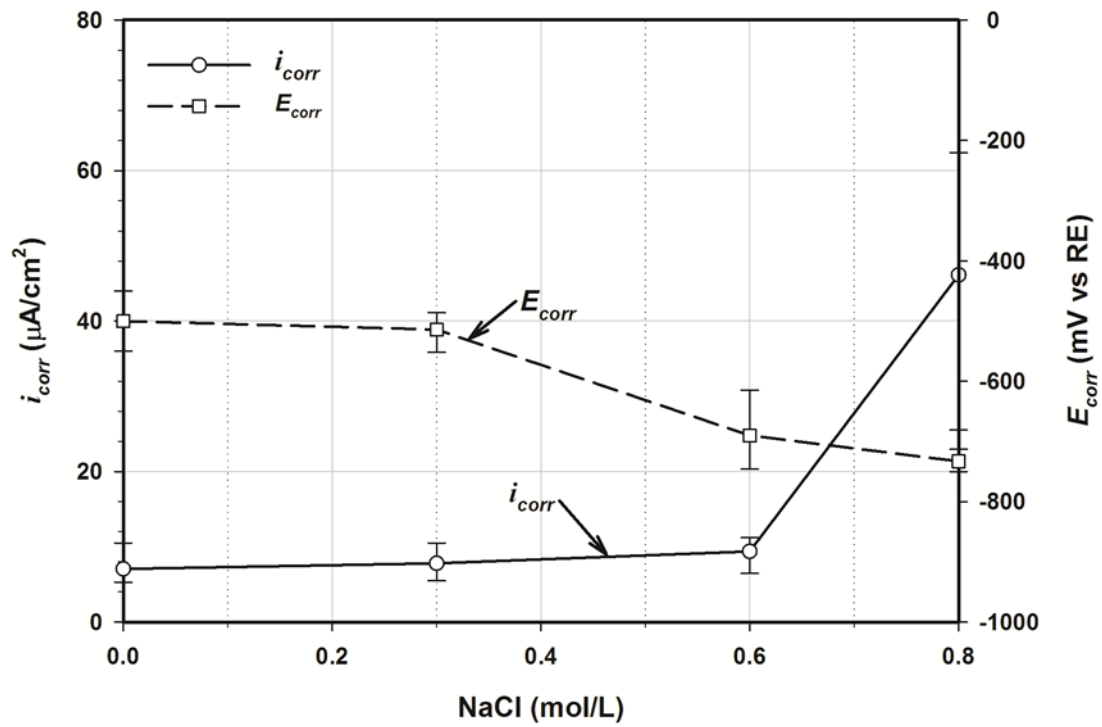

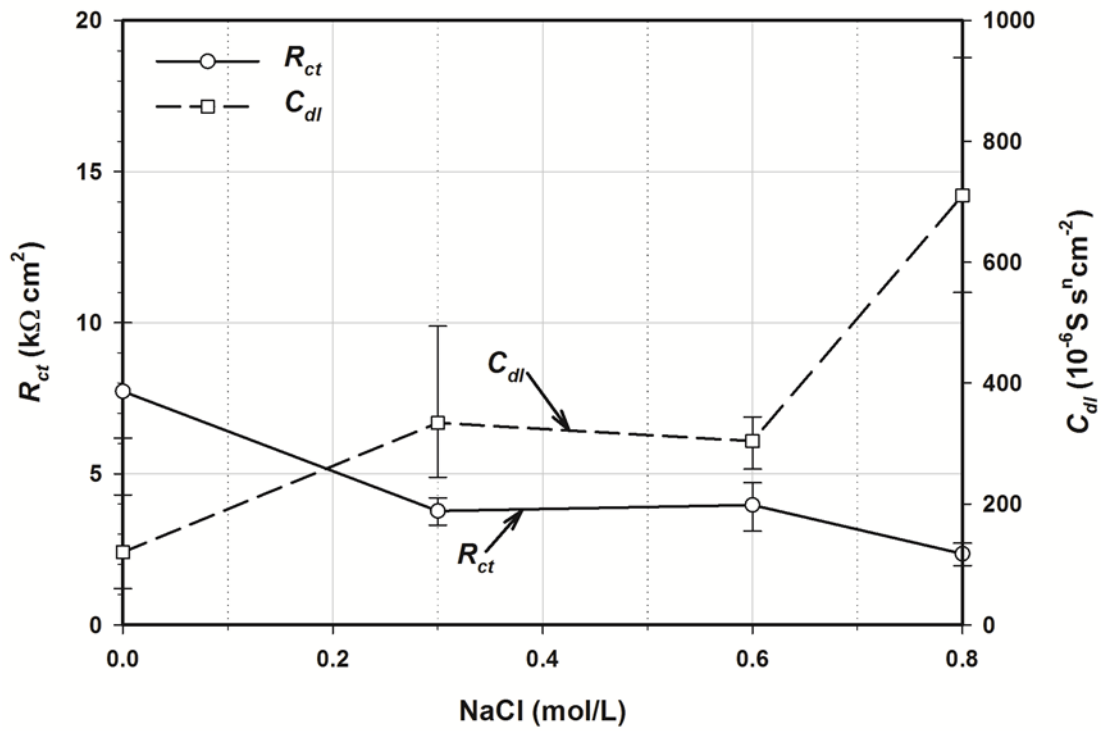Fig. 16. Tafel polarization results (after 10-min stray AC interference)

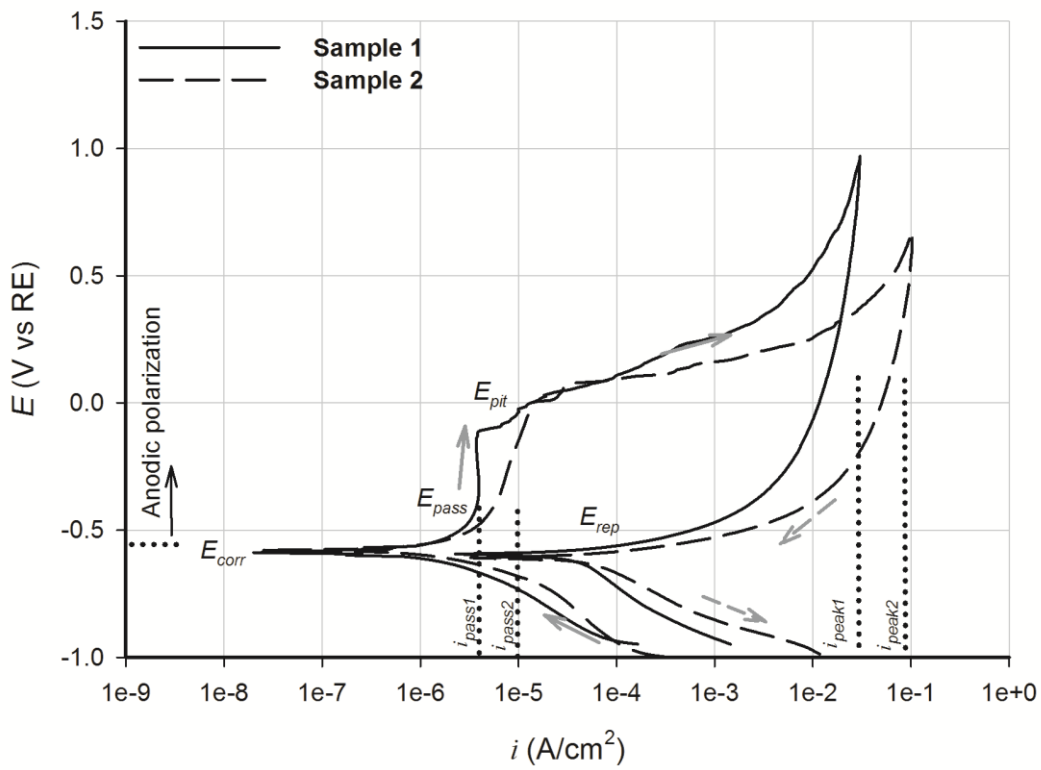Fig. 17. EIS results (after 10-min stray AC interference)

Fig. 18. CP polarization test results (0.3 mol/L NaCl) (after 10-min stray AC interference)

Table 4 EIS best-fit results (after 10-min stray AC interference)

	OCP (mV)	R_s ($\Omega \cdot cm^2$)	R_f ($\Omega \cdot cm^2$)	C_f ($10^{-6} S \cdot s^n \cdot cm^{-2}$)	n_f	R_{ct} ($k\Omega \cdot cm^2$)	C_{dl} ($10^{-6} S \cdot s^n \cdot cm^{-2}$)	n_{dl}
0.0 mol/L NaCl	-210	28.4	24.2	95.5	0.79	7.7	120	0.99
0.3 mol/L NaCl	-474	14.2	52.7	320.0	0.82	3.8	334	0.89
0.6 mol/L NaCl	-720	7.5	15.9	662.4	0.36	3.9	912	0.72
0.8 mol/L NaCl	-724	6.0	38.0	519.7	0.63	2.4	629	0.80

To further study the effect of AC interference at "high" frequencies (e.g. 50 Hz) on the corrosion of steel, a mathematical model was developed based on an electrical circuit model developed for the simulation of the corrosion processes when both anodic and cathodic reactions are under charge-transfer control. In electrical engineering, admittance is usually taken as a measurement of how easy alternating current (AC) flows through a complex circuit. In this work, an electrical circuit seen in Fig. 19, consisting of a resistor (R) in parallel with a capacitor (C), was developed as a simplified model of the admittance of the steel electrolyte interface consisting of a combination of the admittance of the electrical double layer and the charge transfer resistance. Solution resistance was not considered in this model due to the low resistance electrolyte, i.e. saturated $Ca(OH)_2$ solution, used. In such a parallel circuit (Fig. 19), the non-Faradaic current I_1, or capacitive current, does not involve any chemical reactions or charge transfer. It can be said, alternatively, that the variable component of I_1 accounts for the movement of the charged ions (e.g. OH^-, Cl^- or H^+, Na^+ ions) in the electrolyte as well as for the movement of electrons in the metal. These movements compensate for the accumulation or depletion of charges in the interface, namely the "polarization" of the interface occurring as a consequence of the charge transfer imposed by the simulated stray current interference. The charge of the capacitor is directly proportional to its capacitance and the potential difference (E), or:

$$Q = C \cdot E \tag{12}$$

In contrast to I_1, the Faradaic current, I_2, is a direct measure of the rate of the redox reactions. As I_2 is attributable to several redox processes at the interface as discussed previously, the integration of I_2 with respect to time over the half cycles (during which I_2 is anodic) gives a total electrical charge, upon which the corrosion rate (CR) might be qualitatively estimated. In order to achieve the best quantitative calculation of the CR, it is necessary to perform an extended study that can properly discriminate the proportion of the total charge that is attributable to the actual oxidation of the iron. Such a process should involve electrochemical tests in parallel with a direct corrosion assessment (e.g. through a weight loss measurement) and microscopic examination of the samples' surface and cross sections after the test. The latter will help to assess the actual corrosion feature, e.g. generalized or pitting corrosion. There is scope to further develop this process to qualitatively survey the real-time status of a railway's equipment subjected to DC and/or AC interferences. This is an area where on-going research is being conducted.

According to the parallel circuit theory, a larger percentage of the current always flows through the path of lower impedance (Z). For a capacitor, its absolute value ($|Z|$) is inversely proportional to both angular frequency (ω) and capacitance (C).

$$|Z| = \frac{1}{\omega \cdot C} \tag{13}$$

As a result, an increase of the AC angular frequency (ω) and capacitance (C) leads to lower impedance and thus a higher non-Faradaic current (I_1). Consequently, a higher Faradaic current (I_2) is expected with a decrease of ω when the total value of I_1 and I_2 is maintained (galvanostatic). Given such qualitative analysis, the *CR* should therefore be a strong function of ω and this agrees with the previous experimental results [16].
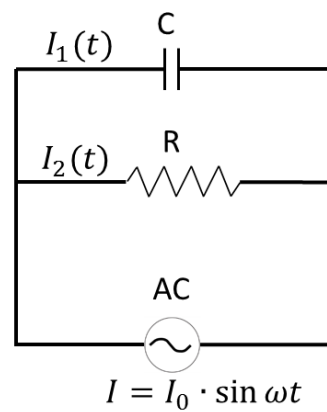

Fig. 19. Equivalent electrical circuit modelling of the steel-electrolyte interface under stray AC interference

The Faradaic current, I_2, was solved and shown as Eq. (14). The calculation and validation processes are presented in the Appendix of this paper.

$$I_2(t) = \frac{I_0}{\sqrt{1+\omega^2 \cdot C^2 \cdot R^2}} \sin(\omega t - \theta) + \frac{\omega \cdot C \cdot R \cdot I_0}{\omega^2 \cdot C^2 \cdot R^2 + 1} \cdot e^{-\frac{t}{C \cdot R}} \tag{14}$$

As discussed in the Appendix, it might be sufficiently accurate to consider the first part of Eq. (14), or Eq. (15), for the prediction of I_2 at a steady state:

$$I_2(t) = \frac{I_0}{\sqrt{1+\omega^2 \cdot C^2 \cdot R^2}} \sin(\omega t - \theta) \tag{15}$$

Eq. (15) allows a quantitative assessment of I_2, which is related to the steel corrosion rate when both the anodic and cathodic reactions are kinetically controlled. This is also subjected to further experimental work assessing whether any anodic reactions other than the primary iron oxidation are attributable to the overall anodic Faradaic current. Eq. (15) indicates that I_2 reduces with an increase of AC frequency and this is in good agreement with the experimental results reported by Wang *et al.* [16]: corrosion current density (i_{corr}) reduced with an increase of AC frequency from 5 to 50 Hz. Eq. (15) also indicates that I_2 is affected by the

combined effect of the admittance of both the electrical double layer (C) and charge transfer resistance (R). Table 2 shows that $C_{dl} \cdot R_{ct}$ reduced with an increase of chloride contents. This could also contribute to the increase of i_{corr} as depicted by Fig. 9.

The mathematical model discussed above takes into account both charge transfer and charge-transfer reactions at the steel-concrete interface. This model provides useful information about the stray AC current-induced steel corrosion rate and its influential factors, based on the kinetic parameters which can be determined by fitting the EIS data with an equivalent electrical circuit. Alongside this, this study shows that equivalent electrical circuit modelling has the potential to allow correlation of stray AC current-induced corrosion damage to experimentally determined kinetics parameter (e.g. C_{dl} and R_{ct}), which paves the way for the development of a real-time railway tunnel health monitoring system.

3.4 Effect of solid electrolyte on the corrosion behaviour of steel fibres under stray AC environments

In order to verify that the results obtained using simulated concrete pore solution were applicable for SFRC, a 4-hr simulated AC stray interference test under the same controlled AC current value (30 mA) was conducted using a 3-electrode cell seen in Fig. 6. EIS was conducted in each hour and results are presented in Fig. 20. Fig. 20 (a) and (c) show that the Bode Phase plots obtained at 0% and 2% NaCl are similar to those obtained using aqueous electrolytes (Fig. 12). As a result, the same equivalent circuit (Fig. 11) was used to model the corrosion processes experienced by the steel fibre embedded in mortar.

In the Bode $|Z|$ plot (Fig. 20 (b)), steel membrane resistance (R_f) and charge transfer resistance (R_{ct}) govern the total impedance ($|Z|$) at low frequencies while R_s is primarily related to the impedance obtained at high frequencies. A small $|Z|$ observed at a high excitation frequency of 10^5 Hz indicates a small solution resistance (R_s). This was confirmed by the best-fit results as seen in Table 5. Membrane resistance (R_f) was found to be much higher than those obtained after the same stray AC interference test but using aqueous electrolytes (Table 4). This indicates that the formation of corrosion products might be more rapid when a solid electrolyte is used according to the previous experimental results [40]. On the other hand, C_f was found to be of a magnitude of 10^{-9} S·s^n·cm^{-2}, indicating that dense corrosion products might have been developed on the steel surface which has a beneficial effect to prevent further corrosion attack. Table 5 also shows that R_{ct} is much greater than those obtained in aqueous electrolytes (Table 2 and Table 4). As R_{ct} is inversely proportional to the *CR*, an enhanced corrosion resistance is expected and this can be attributed to the use of mortar as the electrolyte. Similar to the results obtained using aqueous electrolytes, the presence of chloride (2% by mass of cement) has a detrimental effect on the corrosion resistance of steel fibres: R_{ct} reduced by at least one order of magnitude, indicating high corrosion susceptibility. As R_f is still much less than the charge transfer resistance (R_{ct}), only one time constant is obvious in the Bode Phase plots (Fig. 20 (a) and (c)). In summary, SFRC can develop good corrosion resistance to the stray AC interference under a chloride-free

environment. Special attention is still needed for chloride contaminated SFRC, e.g. ≥ 2% NaCl (by mass of cement).

For comparison purposes, fresh SFRC samples containing 0% and 2% NaCl (by mass of cement) were prepared for a 4-hr simulated stray DC current interference test. A constant DC current of 30 mA was applied between the WE (steel fibre) and CE for 4 hours using the Gamry Interface 1000E potentiostat.

Whether subjected to a simulated stray AC or DC interference, all SFRC samples were transversely cut after the end of the tests. In order to allow the examination of the steel fibre and its interface with the mortar, the cut was at a distance of 1.5 cm from the mid-section of the steel fibre. Fig. 21 shows the cross section of the SFRC specimens. The boundary of corrosion products were highlighted with dashed lines. Serious corrosion of steel fibres was observed in SFRC containing 2% NaCl (by mass of cement) under both AC and DC environments. There was however no sign of corrosion in chloride-free SFRC samples after 4-hr exposure to a stray DC or AC environment, indicating the mitigation effect of a solid electrolyte in absence of NaCl. The effect of solid electrolyte on the quality (nature, structure, physio-chemical properties) of corrosion products developed on the steel surface and volume and/or thickness of the corroded layer, is being investigated using a scanning electron microscope (SEM), equipped with energy disperse x-ray spectroscopy (EDS). This will be discussed in a separate paper.
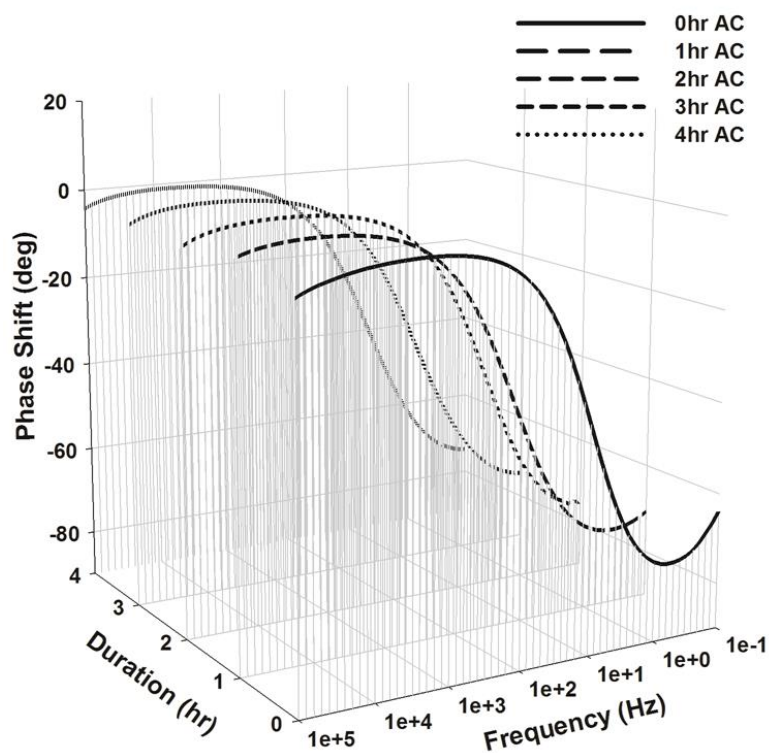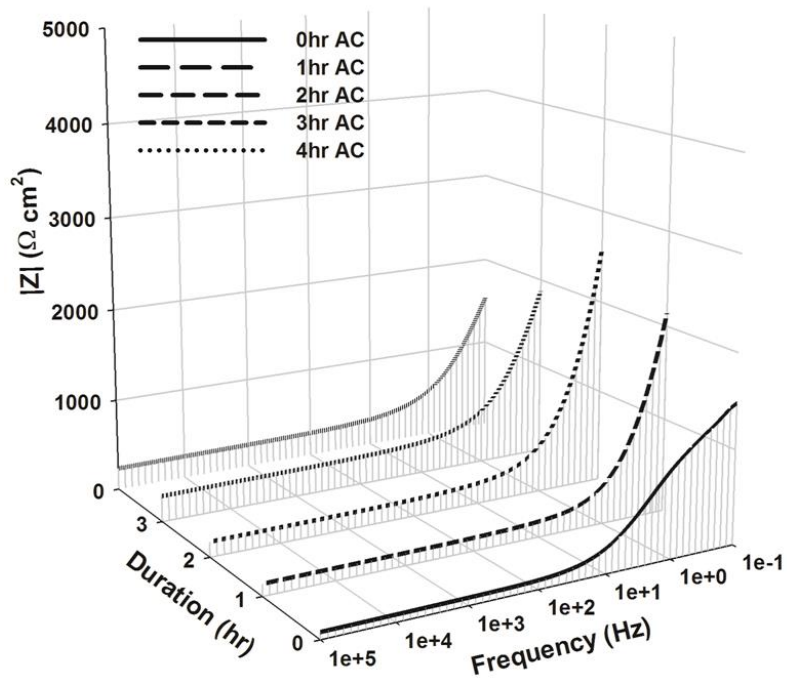

(a) Bode phase plot (0% NaCl SFRC)
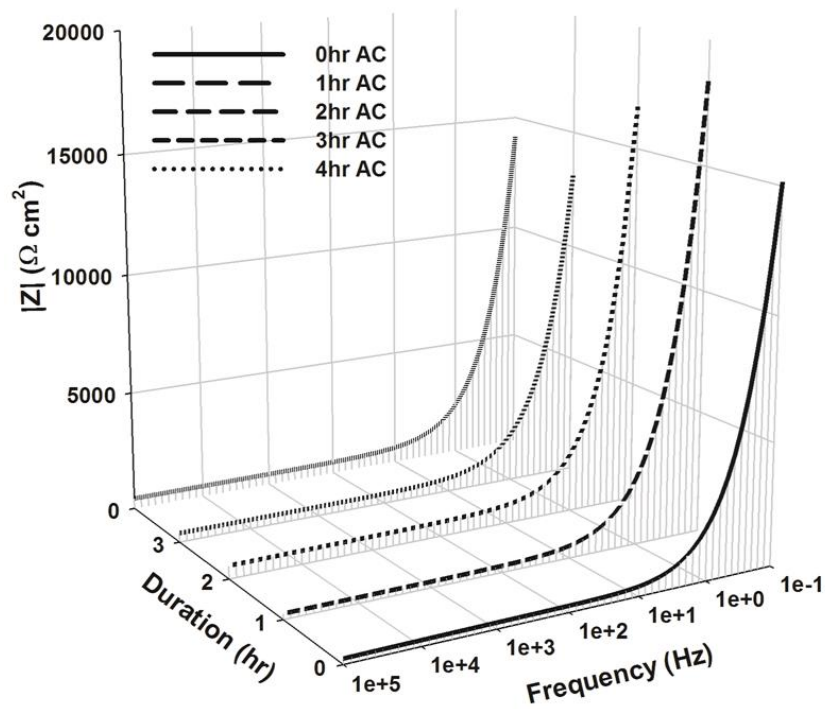
(b) Bode |*Z*| plot (0% NaCl SFRC)
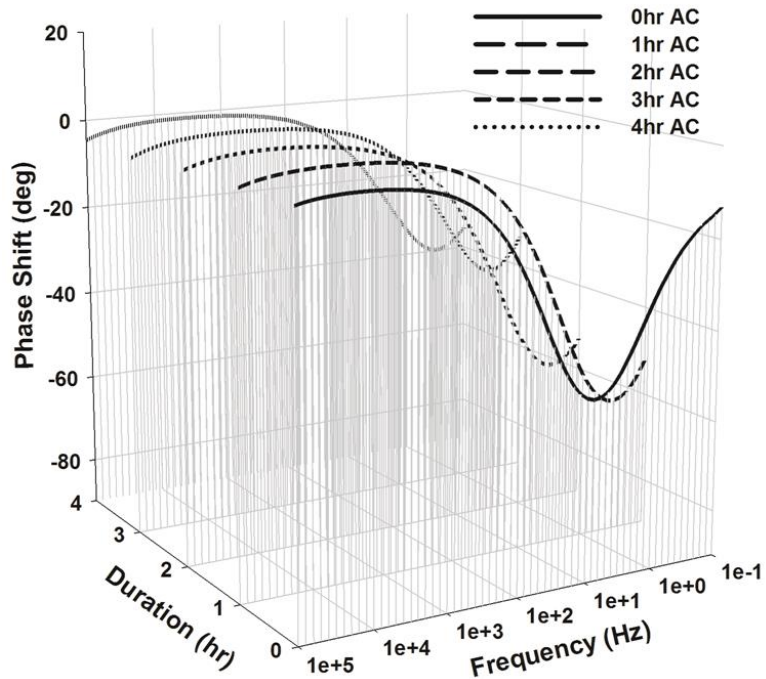
(c) Bode phase plot (2% NaCl SFRC)

(d) Bode |*Z*| plot (2% NaCl SFRC)

Fig. 20. EIS measurements (after 0, 1, 2, 3 and 4-hr AC interference)

(a) 0% NaCl 4-hr **AC**

(b) 2% NaCl 4-hr **AC**

(c) 0% NaCl 4-hr **DC**

(d) 2% NaCl 4-hr **DC**

Fig. 21. Section of SFRC (after 4-hr AC or DC interference)

Table 5 EIS best-fit results (after 0, 1, 2, 3 and 4-hr AC interference)

	OCP	R_s	R_f	C_f	n_f	R_{ct}	C_{dl}	n_{dl}
	(mV)	($\Omega \cdot cm^2$)	($\Omega \cdot cm^2$)	($10^{-9}S \cdot s^n \cdot cm^{-2}$)		($k\Omega \cdot cm^2$)	($10^{-6}S \cdot s^n \cdot cm^{-2}$)	
0% NaCl 0-hr AC	-393.4	2.0	243.7	5.0	0.99	59.9	92.5	0.89
0% NaCl 1-hr AC	-329.0	6.1	243.8	4.3	0.92	70.0	74.3	0.88
0% NaCl 2-hr AC	-324.6	2.4	333.1	4.1	0.69	69.6	88.3	0.87
0% NaCl 3-hr AC	-385.1	1.0	385.6	6.5	0.99	67.8	112.7	0.84
0% NaCl 4-hr AC	-348.1	1.0	458.4	10.1	0.93	70.0	105.0	0.84
2% NaCl 0-hr AC	-540.5	1.0	57.1	8.5	0.99	3.2	303.2	0.77
2% NaCl 1-hr AC	-503.9	1.1	132.4	10.2	0.99	7.8	644.4	0.81
2% NaCl 2-hr AC	-505.1	1.0	171.7	6.0	0.99	6.9	526.4	0.79
2% NaCl 3-hr AC	-557.7	1.0	292.5	7.8	0.99	3.8	657.8	0.71
2% NaCl 4-hr AC	-606.7	1.0	244.7	8.0	0.99	2.7	743.8	0.72

3.5 Ability of discrete steel fibre to pick up and transfer stray AC current

In order to verify that discrete steel fibre can pick up and transfer stray AC current, a 24-hr stray AC interference test (Fig. 7) was conducted under a controlled AC current value (10 mA, 50 Hz). The voltage drop (E) between the steel fibre and auxiliary graphite plate is presented in Fig. 22. It shows that E increases with time in absence of NaCl, showing increased impedance and possible enhanced corrosion resistance which can be attributed to the maturity of mortar alongside the cement hydration reactions [41]. A combined effect of AC currents and 2% NaCl (% by mass of cement) however led to a constant reduction in E, indicating reduced impedance alongside possible enhanced corrosion.

After the 24-hr simulated stray AC current interference test, EIS was conducted to the embedded steel fibre. EIS results are presented as the Bode phase plot (Fig. 23 (a)), Bode $|Z|$ plot (Fig. 23 (b)) and Nyquist plot (Fig. 23 (c)). In the Bode $|Z|$ plot (Fig. 23 (b)), an increased $|Z|$ is observed without the presence of NaCl. Consequently, an increased voltage (E) is required to drive the AC current through, just as Fig. 22 indicates. Fig. 23 (a) shows that the phase angle (θ) drops gradually at low frequencies, especially under a combined effect of NaCl and AC interference which shifts θ downwards drastically, indicating that the steel passive layer might have been locally destroyed and the diffusion process might have become a governing factor controlling the overall corrosion rate according to the previous experimental results [23]. Fig. 23 (a) shows that the Bode Phase plots are very similar to Fig. 12 (a). As a result, the same equivalent circuit (Fig. 11) was used to model the corrosion processes experienced by the embedded steel fibre. The EIS best-fit results are shown in Table 6. After the 24-hr simulated stray AC current interference, R_{ct} under a chloride-free condition (0% NaCl) is 92.9 $k\Omega \cdot cm^2$ which is much higher than that obtained under a combined effect of 2% NaCl (by mass of cement), 7.9 $k\Omega \cdot cm^2$. The latter is still higher than the SFRC specimen subjected to a bigger amplitude AC current perturbation (30 mA) but of a shorter duration (4 hrs), as seen in Table 5. This shows the necessity of considering both the amplitude of stray currents and duration when assessing the severity related to stray current

attack. In summary, a discrete steel fibre embedded in concrete can pick up stray AC currents but it still demonstrates good corrosion resistance to the AC interference under a chloride-free environment. Special attention is still needed for SFRC subjected to high concentration chloride, e.g. ≥ 2% NaCl (by mass of cement). This work also shows that AC interference at "high" frequencies (e.g. 50 Hz), which is same as the National Grid AC frequency and used in electrified railway, has a detrimental effect on the corrosion resistance of SFRC.
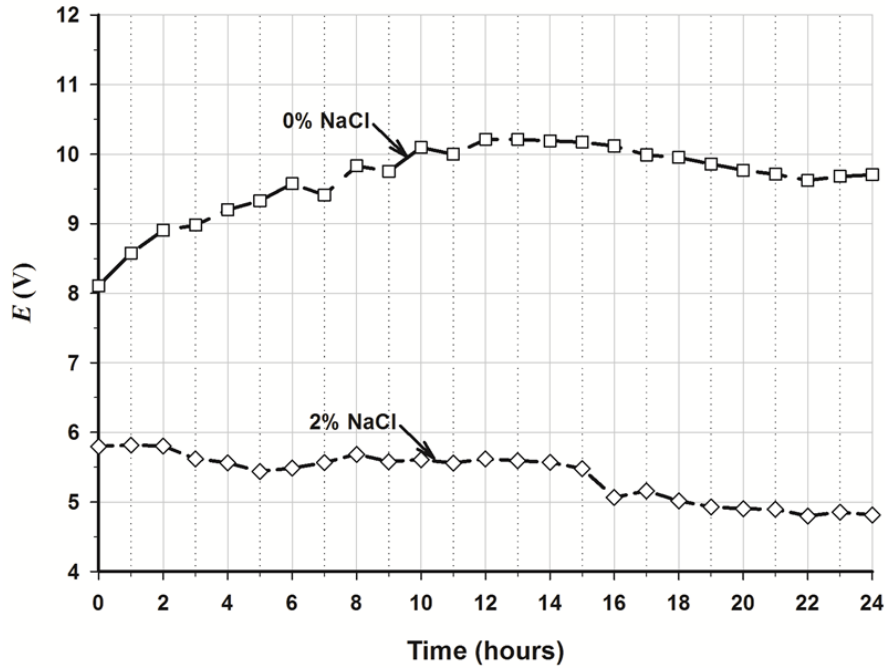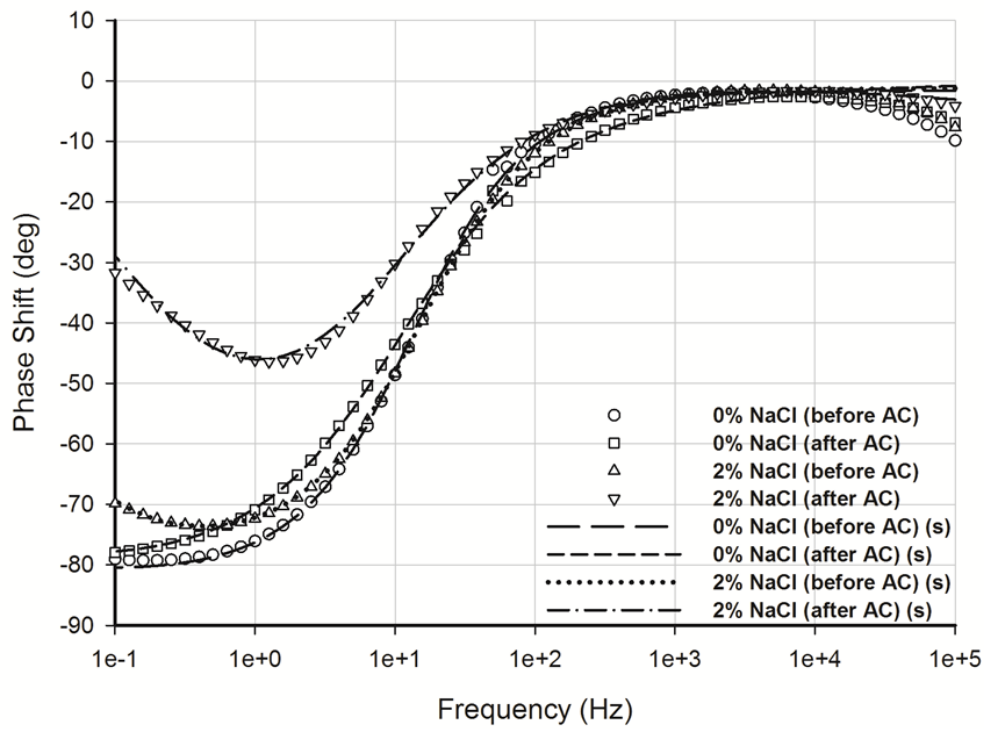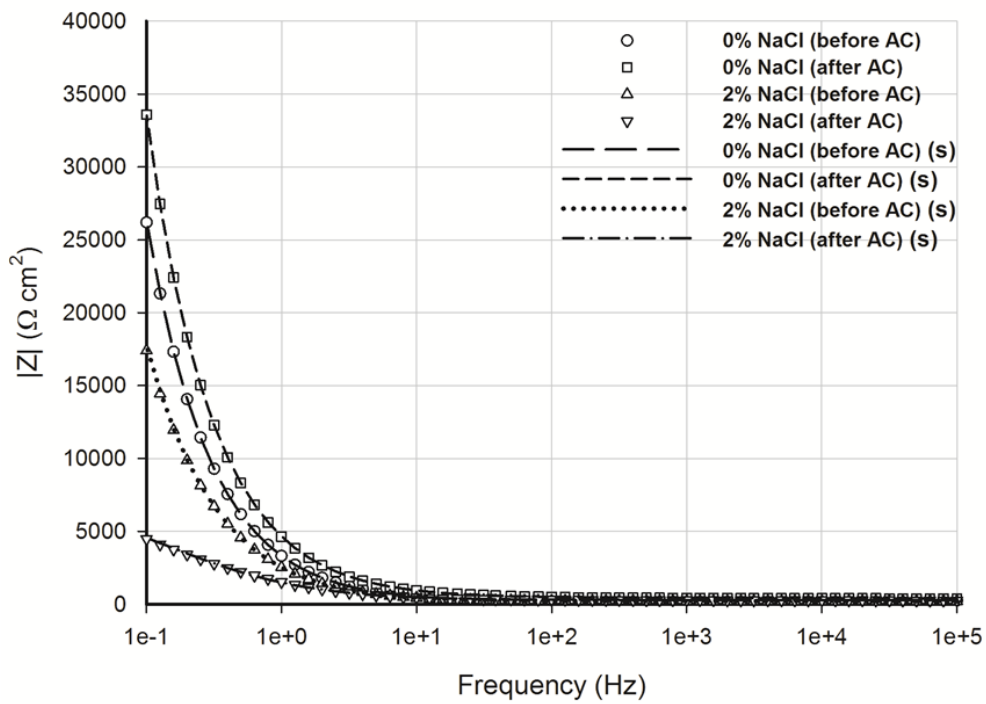

Fig. 22. Effect of chloride contents on the ability that discrete steel fibre to pick up stray AC currents ($I_0 = 10mA;\ \omega = 50\ Hz$)
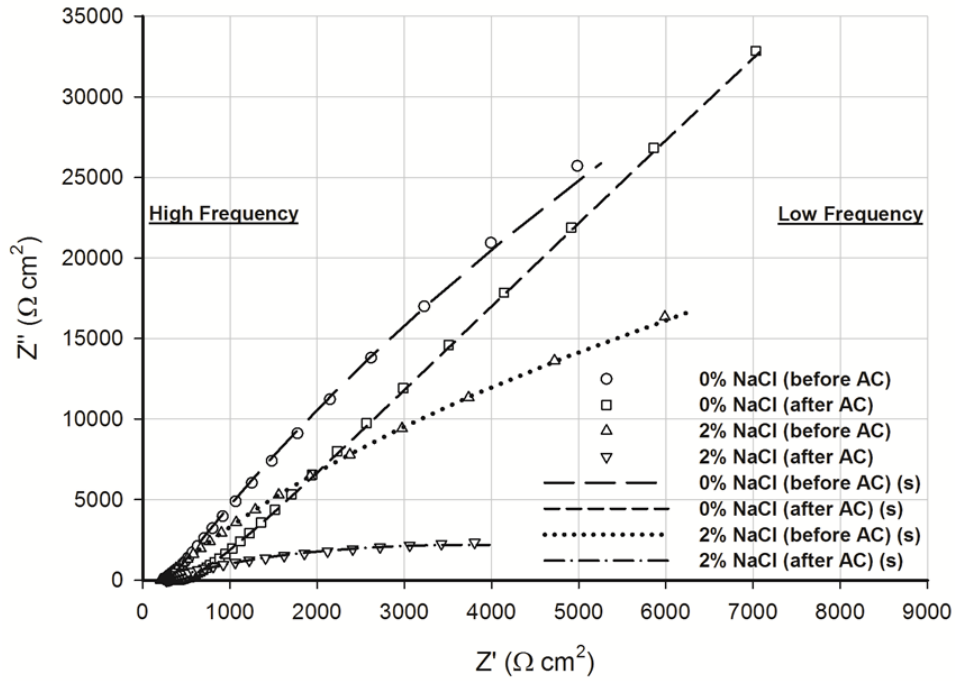
(a) Bode Phase plot

(b) Bode Z plot

(c) Nyquist plot

Fig. 23. EIS results (after 24-hr simulated stray AC current interference)

Table 6 EIS best-fit results (before and after 24-hr simulated stray AC current interference)

	OCP (mV)	R_s ($\Omega\cdot cm^2$)	R_f ($\Omega\cdot cm^2$)	C_f ($10^{-9}S\cdot s^n\cdot cm^{-2}$)	n_f	R_{ct} ($k\Omega\cdot cm^2$)	C_{dl} ($10^{-6}S\cdot s^n\cdot cm^{-2}$)	n_{dl}
0% NaCl (before)	-296	29.0	280	10	0.56	85.0	58.1	0.89
0% NaCl (after)	-311	37.4	271	17	0.89	92.9	46.7	0.85
2% NaCl (before)	-310	52.1	163	91	0.87	14.4	82.6	0.86
2% NaCl (after)	-593	44.3	213	100	0.64	7.9	183.8	0.72

4. Conclusion

The stray current induced corrosive damage to railway infrastructure will become more prominent in the UK as the government is committed to developing more electrified rail networks. The effects of stray AC and DC interferences on the corrosion of steel fibres were investigated by three instrumental methods for electrochemistry:

1) Tafel polarization and EIS provides useful information about electrochemical kinetics relating to the corrosion rate where the values of polarization are low.

2) Cyclic potentiodynamic (CP) polarization results, especially those obtained at a high-value anodic overpotential, provides useful information which can be used to quantitatively assess the corrosion behaviour of steel fibres subjected to a simulated stray DC interference.

The experimental results indicate that steel fibres have a high inherent corrosion resistance to either AC or DC interference (30 mA) under a chloride-free condition. The presence of a small amount of NaCl, i.e. 0.3 mol/L in the concrete pore solution or 2% by mass of cement, however greatly enhances steel fibre corrosion. In comparison to stray AC, chlorides have a greater detrimental effect on the corrosion resistance of steel fibres, despite the use of solid electrolytes such as mortar may have a mitigation effect. The analytical model proposed in this work also shows promising results that open the way to the development of a real-time railway tunnel health monitoring system based on the electrical element parameters (e.g. R_{ct} and C_{dl}) measurements.

5. Further study outlook

Positive and negative cycles involved into a stray AC allow both anodic and cathodic reactions to take place on the steel surface. Cathodic reactions (e.g. Eq. (10) and (11)) as experienced in negative AC circles can lead to an increase in pH due to the OH$^-$ ions generated and accumulated. This may become prominent when concrete, which has a stable microstructure, is used as the electrolyte. Previous studies related to the stray AC current-induced corrosion of underground steel pipelines coated and cathodically protected (owing to the electrical coupling between AC electric power transmission lines or AC powered railways and the cathodically protected pipelines) reported that the presence of the DC cathodic protection together with an AC interference may have specific impacts on the corrosion behaviour of these components [42]. More specifically, the normal increase of the soil pH adjacent to the steel pipelines due to the DC cathodic polarization of the interface may lead, in presence of the AC interference and depending on the operating conditions of the pipeline and the AC interference features, to further increase of the local pH and this can be taken as a specific situation of AC corrosion (autocatalytic) in nature. These situations have required, in the domain of operation of these underground pipelines, the development of specific cathodic protection criteria, i.e. non-conventional with respect to the criteria in use in absence of AC interferences.

6. Appendix

Fig. 19 represents a simplified equivalent electrical circuit of the steel-concrete interfacial electrochemical reactions under stray AC interference, assuming an electrolyte resistance of negligible value compared with the impedance values of the other components of the circuit, i.e. a constant charge transfer resistance (R) connected in parallel with a constant capacitance (C) representing the interfacial double layer. The sum of the instantaneous currents through each path, I_1 and I_2, is equal to the total current (I). The above processes can be represented as:

$$R_{ct} \cdot I_2(t) = \frac{1}{C} \int I_1 dt \tag{A1}$$

$$I_1(t) + I_2(t) = I = I_0 \cdot \sin \omega t \tag{A2}$$

Taking differentiation with respect to t, Eq. (A1) becomes:

$$R_{ct} \cdot I_2'(t) = \frac{I_1}{C} \tag{A3}$$

Eq. (A3) can be written as:

$$I_1(t) = C \cdot R \cdot I_2'(t) \tag{A4}$$

In conjunction with Eq. (A2), $I_2(t)$, the Faradaic current through the resistor can be presented as:

$$I_2'(t) + \frac{1}{C \cdot R} I_2(t) = \frac{I_0 \cdot \sin \omega t}{C \cdot R} \tag{A5}$$

Eq. (A5) is shown below as a nonhomogeneous ordinary differential equation (ODE):

$$y' + a \cdot y = b \sin \omega t \tag{A6}$$

Where $y = I_2(t)$, $a = \frac{1}{C \cdot R}$ and $b = \frac{I_0}{C \cdot R}$.

Eq. (A7) represents the homogeneous ordinary differential equation associated to Eq. (A6):

$$y' + a \cdot y = 0 \tag{A7}$$

Eq. (A7) can be written as:

$$\frac{dy}{y} = -a \cdot dt \tag{A8}$$

Which can be solved by integration as:

$$lny = -at + lnc \tag{A9}$$

Where c is the constant of integration. Taking exponents on both sides

$$y = ce^{-at} \tag{A10}$$

It is known that the solutions of the non-homogeneous Eq. (A6) can be obtained by considering that c is a function of t. Let $c = u(t)$ and Eq. (A10) becomes

$$y = u(t) \cdot e^{-at} \tag{A11}$$

Taking differentiation on both sides

$$y' = u'(t) \cdot e^{-at} - a \cdot u(t) \cdot e^{-at} \tag{A12}$$

Substitution of Eq. (A11) and (A12) into (A6)

$$u' = b \cdot e^{at} \cdot \sin \omega t \tag{A13}$$

By integration

$$u = b \int e^{at} \cdot \sin \omega t \, dt + d \tag{A14}$$

Where d is the constant of integration of Eq. (A14). Taking integration by parts, Eq. (A14) can be solved as:

$$u = \frac{b \cdot e^{at}}{\omega^2 + a^2} (a \cdot \sin \omega t - \omega \cdot \cos \omega t) + d \tag{A15}$$

By substituting Eq. (A15) into (A11), the general solution of Eq. (A6) is

$$y = \frac{b}{\omega^2 + a^2} (a \cdot \sin \omega t - \omega \cdot \cos \omega t) + d \cdot e^{-at} \tag{A16}$$

Applying the initial condition, $y|_{t=0} = 0$, d can be solved as:

$$d = \frac{b \cdot \omega}{\omega^2 + a^2} \tag{A17}$$

Eq. (A16) therefore becomes:

$$y = \frac{b}{\omega^2 + a^2} (a \cdot \sin \omega t - \omega \cdot \cos \omega t) + \frac{b \cdot \omega}{\omega^2 + a^2} \cdot e^{-at} \tag{A18}$$

Eq. (A18) can be further simplified as:

$$y = \frac{b}{\sqrt{\omega^2 + a^2}} \sin(\omega t - \theta) + \frac{b \cdot \omega}{\omega^2 + a^2} \cdot e^{-at} \tag{A19}$$

Where $\theta = arctan \frac{\omega}{a}$, the phase drift (rads).

As $y = I_2(t)$, $a = \frac{1}{C \cdot R}$ and $b = \frac{I_0}{C \cdot R}$, the solution of the initial problem is:

$$I_2(t) = \frac{I_0}{\sqrt{1 + \omega^2 \cdot C^2 \cdot R^2}} \sin(\omega t - \theta) + \frac{\omega \cdot C \cdot R \cdot I_0}{\omega^2 \cdot C^2 \cdot R^2 + 1} \cdot e^{-\frac{t}{C \cdot R}} \tag{A20}$$

The validity of Eq. (A20) was assessed using an electrical circuit shown in Fig. 24. It consists of a standard resistor and capacitor. AC current $I_0 \cdot \sin \omega t$ ($I_0 = 10 \, mA$; $f = 50Hz$; $\omega = 2\pi f$) was swept through this circuit using the Gamry Interface 1000E potentiostat. The potential drop between the resistor ends was captured by the potentiostat to calculate I_2 according to Ohm's law. The predicted I_2 according to Eq. (A20) was in good agreement with the experimental measurements as seen in Fig. 25. Alongside this, the theoretical model also indicates that the second part of Eq. A20 reduces to < 0.1 mA in only 0.0085 seconds. It is therefore accurate enough to consider the first part of Eq. (A20) for the prediction of I_2 at a steady state.
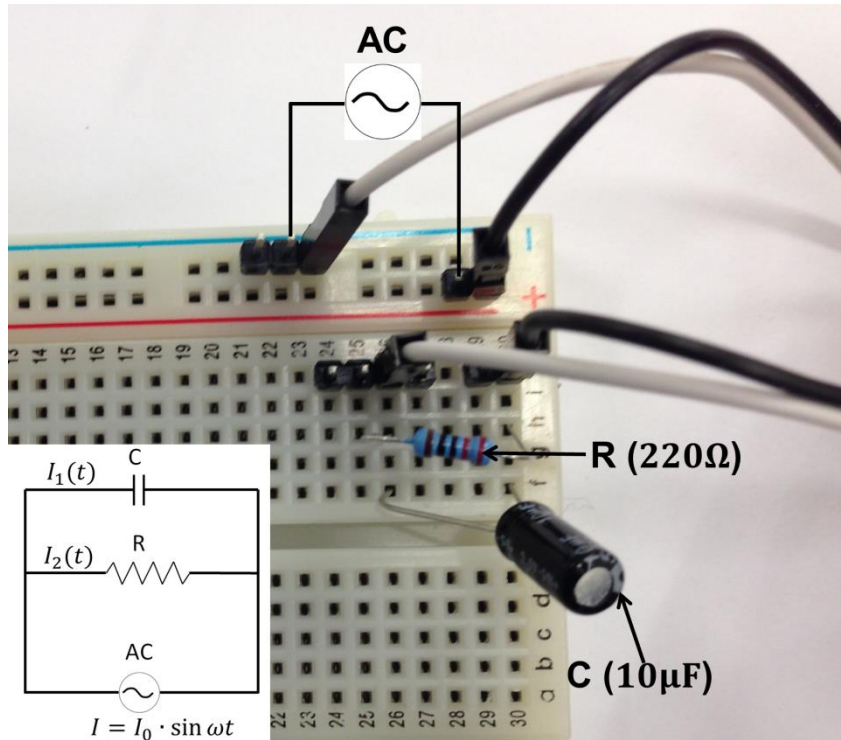
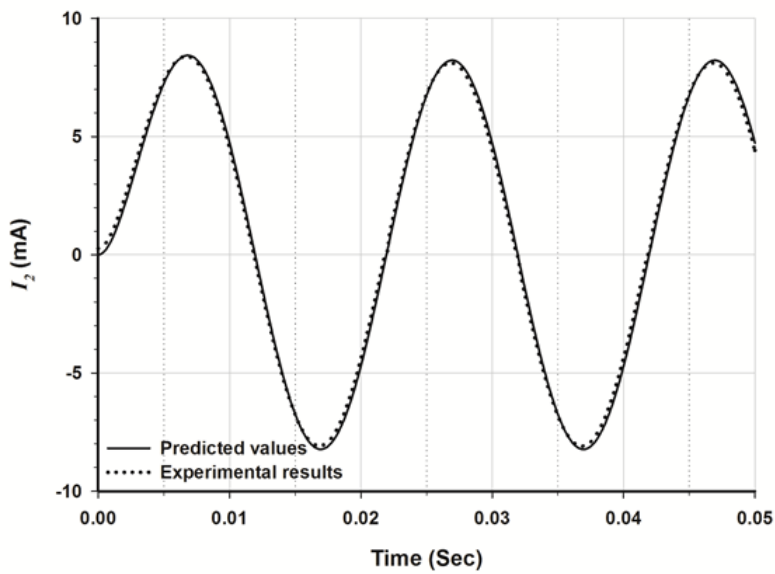Fig. 24. Electronic components used for modelling the electrical circuit (Fig. 19)

Fig. 25. Predicted and measured I_2 values

References

[1] Crossrail, Europe's largest construction project. http://www.crossrail.co.uk/construction/, 2017 (accessed 27/6/2017).

[2] Railway-technology, High Speed 2 (HS2) railway. http://www.railway-technology.com/projects/high-speed-2-hs2/, 2017 (accessed 27/6/2017).

[3] K. Tang, Stray current induced corrosion to steel fibre reinforced concrete, Cement and Concrete Research, 100 (2017) 445-456.

[4] J. Hudson, Comprehensive rock engineering, Pergamon Press, Oxford, UK, 1993.

[5] A. Steel, Design standards stray current management, Office of Rail Regulation.

[6] R. Kemp, Traction energy metrics, Rail Safety and Standards Board, Lancaster University, UK, 2007.

[7] P. Keen, R. Phillpotts, Low cost electrification for branch lines, DeltaRail, Derby, 2010.

[8] BSI, BS EN 15280:2013 Evaluation of A.C. corrosion likelihood of buried pipelines applicable to cathodically protected pipelines, British Standards Institution, 2013.

[9] L. Bertolini, M. Carsana, P. Pedeferri, Corrosion behaviour of steel in concrete in the presence of stray current, Corrosion Science, 49 (2007) 1056-1068.

[10] D. Kuang, Y.F. Cheng, Understand the AC induced pitting corrosion on pipelines in both high pH and neutral pH carbonate/bicarbonate solutions, Corrosion Science, 85 (2014) 304-310.

[11] A. Brenna, S. Beretta, F. Bolzoni, M. Pedeferri, M. Ormellese, Effects of AC-interference on chloride-induced corrosion of reinforced concrete, Construction and Building Materials, 137 (2017) 76-84.

[12] H.R. Hanson, J. Smart, AC Corrosion on a Pipeline Located in a HVAC Utility Corridor, in: Corrosion, NACE International, New Orleans, Louisiana, 2004.

[13] C. Cao, Principles of electrochemistry of corrosion, Chemical industry Press, Beijing, China, 2008.

[14] S.B. Lalvani, X. Lin, A revised model for predicting corrosion of materials induced by alternating voltages, Corrosion Science, 38 (1996) 1709-1719.

[15] R.W. Bosch, W.F. Bogaerts, A theoretical study of AC-induced corrosion considering diffusion phenomena, Corrosion Science, 40 (1998) 323-336.

[16] L.W. Wang, X.H. Wang, Z.Y. Cui, Z.Y. Liu, C.W. Du, X.G. Li, Effect of alternating voltage on corrosion of X80 and X100 steels in a chloride containing solution – Investigated by AC voltammetry technique, Corrosion Science, 86 (2014) 213-222.

[17] S. Goidanich, L. Lazzari, M. Ormellese, AC corrosion – Part 1: Effects on overpotentials of anodic and cathodic processes, Corrosion Science, 52 (2010) 491-497.

[18] C. Wen, J. Li, S. Wang, Y. Yang, Experimental study on stray current corrosion of coated pipeline steel, Journal of Natural Gas Science and Engineering, 27 (2015) 1555-1561.

[19] S.O. Engblom, J.C. Myland, K.B. Oldham, Must ac voltammetry employ small signals?, Journal of Electroanalytical Chemistry, 480 (2000) 120-132.

[20] S.O. Engblom, J.C. Myland, K.B. Oldham, A.L. Taylor, Large Amplitude AC Voltammetry - A Comparison Between Theory and Experiment, Electroanalysis, 13 (2001) 626-630.

[21] J. Wang, Analytical electrochemistry, Wiley-VCH, New York, USA, 2000.

[22] Metrohm, Autolab application note EIS01: electrochemical impedance spectroscopy (EIS). http://www.ecochemie.nl/Applications/, 2011 (accessed 1/12/2016).

[23] J. Wei, X.X. Fu, J.H. Dong, W. Ke, Corrosion evolution of reinforcing steel in concrete under dry/wet cyclic conditions contaminated with chloride, Journal of Materials Science and Technology, 28 (2012) 905-912.

[24] S. Goidanich, L. Lazzari, M. Ormellese, AC corrosion - Part 2: Parameters influencing corrosion rate, Corrosion Science, 52 (2010) 916-922.

[25] S. Patil, B. Karkare, S. Goyal, Corrosion induced damage detection of in-service RC slabs using acoustic emission technique, Construction and Building Materials, 156 (2017) 123-130.

[26] H. Sadeghi-Pouya, E. Ganjian, P. Claisse, K. Muthuramalingam, Corrosion durability of high performance steel fibre reinforced concrete, in: T.N. Peter Claisse (Ed.) The 3rd international conference on sustainable construction materials and technologies, Kyoto, Japan, 2013.

[27] S.J. Duranceau, W.J. Johnson, R.J. Pfeiffer-Wilder, A study examining the effect of stray current on the integrity of continuous and discontinuous reinforcing bars, Experimental Techniques, 35 (2011) 53-58.

[28] K. Wang, Q.S. Wu, M.C. Chen, L. Xie, Corrosion fatigue of reinforced concrete in the presence of stray current, in: 2011 International Conference on Electric Technology and Civil Engineering (ICETCE), 2011, pp. 1133-1136.

[29] W. Li, The monitor and control system of stray current corrosion in metro, Urban mass transit, 6 (2003) 48-52.

[30] A. Yadav, Traction choices: overhead ac vs third rail dc, International Railway Journal, Feb (2013).

[31] BSI, BS EN 50122-2:2010 Railway applications - fixed installations - electrical safety, earthing and the return circuit, British Standards Institution, 2010.

[32] C.A. Charalambous, I. Cotton, P. Aylott, N.D. Kokkinos, A Holistic Stray Current Assessment of Bored Tunnel Sections of DC Transit Systems, IEEE Transactions on Power Delivery, 28 (2013) 1048-1056.

[33] C.Q. Ye, R.G. Hu, S.G. Dong, X.J. Zhang, R.Q. Hou, R.G. Du, C.J. Lin, J.S. Pan, EIS analysis on chloride-induced corrosion behavior of reinforcement steel in simulated carbonated concrete pore solutions, Journal of Electroanalytical Chemistry, 688 (2013) 275-281.

[34] J. Shi, W. Sun, J. Jiang, Y. Zhang, Influence of chloride concentration and pre-passivation on the pitting corrosion resistance of low-alloy reinforcing steel in simulated concrete pore solution, Construction and Building Materials, 111 (2016) 805-813.

[35] Gamry, Gamry Echem Analyst in, Gamry Instruments, Inc., 2015.

[36] M. Saremi, E. Mahallati, A study on chloride-induced depassivation of mild steel in simulated concrete pore solution, Cement and Concrete Research, 32 (2002) 1915-1921.

[37] P.R. Roberge, Corrosion engineering: principles and practice, McGraw-Hill, 2008.

[38] Concrete Society, Technical Report 44 Relevance of cracking in concrete to reinforcement corrosion, 2 ed., Concrete Society, Surrey, UK, 2015.

[39] D.-T. Chin, P. Sachdev, Corrosion by alternating current: polarization of mild steel in neutral electrolytes, Electrochemical science and technology, 130 (1983) 1714-1718.

[40] Z.X. Yang, B. Kan, J.X. Li, Y.J. Su, L.J. Qiao, Hydrostatic pressure effects on corrosion behavior of X70 pipeline steel in a simulated deep-sea environment, Journal of Electroanalytical Chemistry, 822 (2018) 123-133.

[41] K. Tang, S. Wilkinson, G. Beattie, Effects of curing temperature on the hydration of GGBS blended concrete and the use of electron microscope particle analysis Advances in Cement Research, 29 (2017) 322-335.

[42] A.Q. Fu, F.Y. Cheng, F.Y. Cheng, Effect of alternating current on corrosion and effectiveness of cathodic protection of pipelines, Canadian Metallurgical Quarterly, 51 (2012) 81-90.